

1 **Specialized metabolism by trichome-preferentially-expressed Rubisco and fatty acid**  
2 **synthase components**

3

4 Wangming Ji<sup>1†</sup>, Sabyasachi Mandal<sup>1†</sup>, Yohannes H. Rezenom<sup>2</sup>, Thomas D. McKnight<sup>1,\*</sup>

5

6 <sup>1</sup> Department of Biology, Texas A&M University, College Station, Texas 77843, USA

7 <sup>2</sup> Department of Chemistry, Texas A&M University, College Station, Texas 77843, USA

8

9 † These authors contributed equally to the paper.

10

11 \* Senior author and author for correspondence: [mcknight@bio.tamu.edu](mailto:mcknight@bio.tamu.edu)

12

13 ORCID IDs: 0000-0003-0694-2472 (W.J.); 0000-0001-6093-3468 (S.M.); 0000-0002-9990-4784

14 (Y.H.R.); 0000-0002-9863-2035 (T.D.M.)

15

16 **Short running head:** Trichome acylsugar metabolism by Rubisco and FAS

17

18 The author responsible for distribution of materials integral to the findings presented in this  
19 article in accordance with the policy described in the Instructions for Authors

20 (<https://academic.oup.com/plphys/pages/general-instructions>) is Thomas D. McKnight

21 ([mcknight@bio.tamu.edu](mailto:mcknight@bio.tamu.edu)).

22

23

24

25 **Abstract**

26 Acylsugars, specialized metabolites with defense activities, are secreted by trichomes of many  
27 solanaceous plants. Several acylsugar metabolic genes (AMGs) remain unknown. We previously  
28 reported multiple candidate AMGs. Here, using multiple approaches, we characterized additional  
29 AMGs. First, we identified differentially expressed genes between high- and low-acylsugar-  
30 producing F<sub>2</sub> plants derived from a cross between *Solanum lycopersicum* and *S. pennellii*, which  
31 produce acylsugars ~1% and ~20% of leaf dry weight, respectively. Expression levels of many  
32 known and candidate AMGs positively correlated with acylsugar amounts in F<sub>2</sub> individuals.  
33 Next, we identified *lycopersicum-pennellii* putative orthologs with higher nonsynonymous to  
34 synonymous substitutions. These analyses identified four candidate genes, three of which  
35 showed enriched expression in stem trichomes compared to underlying tissues (shaved stems).  
36 Virus-induced gene silencing confirmed two candidates, *Sopen05g009610* [beta-ketoacyl-(acyl-  
37 carrier-protein) reductase; fatty acid synthase component] and *Sopen07g006810* (Rubisco small  
38 subunit), as AMGs. Phylogenetic analysis indicated that *Sopen05g009610* is distinct from  
39 specialized metabolic cytosolic reductases, but closely related to two capsaicinoid biosynthetic  
40 reductases, suggesting evolutionary relationship between acylsugar and capsaicinoid  
41 biosynthesis. Additionally, data mining revealed that orthologs of *Sopen05g009610* are  
42 preferentially expressed in trichomes of several acylsugar-producing solanaceous species.  
43 Similarly, orthologs of *Sopen07g006810* were identified as trichome-preferentially-expressed  
44 members, which form a phylogenetic clade distinct from those of mesophyll-expressed “regular”  
45 Rubisco small subunits. Furthermore,  $\delta^{13}\text{C}$  analyses indicated recycling of metabolic CO<sub>2</sub> into  
46 acylsugars by *Sopen07g006810* and shed light on how trichomes support high levels of  
47 specialized metabolite production. These findings have implications for genetic manipulation of  
48 trichome specialized metabolism in solanaceous crops, including tomato, potato, and tobacco.

49

50

51

52

53

## 54 **Introduction**

55 Plant metabolites are traditionally classified into primary or central metabolites and secondary or  
56 specialized metabolites. In contrast to evolutionarily conserved primary metabolites, specialized  
57 metabolites are found in specific taxonomic groups and exhibit greater structural diversity. The  
58 building blocks of specialized metabolites are derived from products of primary metabolism; for  
59 example, alkaloids are derived from amino acids, whereas acylsugars are derived from sugar and  
60 fatty acids. The evolution of a specialized metabolic pathway requires evolution of new gene  
61 functions, which can be achieved through a variety of mechanisms, including duplication of  
62 primary metabolic genes followed by neo- or sub-functionalization and/or changes in spatio-  
63 temporal gene expression (Moghe and Last, 2015).

64 Specialized metabolites have important roles in plant-environment interactions. For  
65 example, acylsugars, which are nonvolatile and viscous metabolites secreted through glandular  
66 trichomes of many species in the Solanaceae (Slocombe et al., 2008; Moghe et al., 2017),  
67 provide protection against biotic and abiotic stress. These compounds contribute directly and  
68 indirectly to plant defense by providing resistance against insect herbivores (Alba et al., 2009;  
69 Leckie et al., 2016), by mediating multitrophic defense by attracting predators of herbivores  
70 through volatile short-chain aliphatic acids produced from acylsugar breakdown (Weinhold and  
71 Baldwin, 2011), and by protecting plants from microbial pathogens (Luu et al., 2017).  
72 Acylsugars also protect plants from desiccation (Fobes et al., 1985; Feng et al., 2021). These  
73 beneficial properties have led to interests in understanding acylsugar metabolism and identifying  
74 factors that control their production for breeding agronomically important crops with better  
75 resistance against insect herbivores (Bonierbale et al., 1994; Lawson et al., 1997; Leckie et al.,  
76 2012).

77 Acylsugars exhibit tremendous structural variation in the Solanaceae. Both branched- and  
78 straight-chain fatty acids are esterified to the sugar moiety (glucose or sucrose) to form  
79 acylsugars, and major acyl chains vary in length (C2 to C12) in different species (Kroumova et  
80 al., 2016; Moghe et al., 2017). Predominant branched-chain fatty acids include 2-  
81 methylpropanoate, 3-methylbutanoate, and 2-methylbutanoate, which are derived from  
82 branched-chain amino acids (valine, leucine, and isoleucine, respectively) (Walters and Steffens,  
83 1990). Branched medium-chain acyl groups, such as 6-methylheptanoate and 8-methylnonanoate,

84 are derived from branched short-chain precursors through elongation reactions mediated by  
85 either  $\alpha$ -ketoacid (one-carbon elongation) or fatty acid synthase (FAS; two-carbon elongation)  
86 (Kroumova and Wagner, 2003). Predominant straight-chain fatty acids, such as *n*-decanoate and  
87 *n*-dodecanoate, are presumably derived from acetyl-CoA via FAS-mediated *de novo* biosynthesis  
88 (Walters and Steffens, 1990; Mandal et al., 2020). Once acyl chains are produced, specific sets of  
89 acylsugar acyltransferases (ASATs) in different species of the Solanaceae attach these aliphatic  
90 groups to different carbon positions of the sugar moiety, leading to remarkable metabolic  
91 diversity (Schilmiller et al., 2015; Fan et al., 2016; Moghe et al., 2017; Nadakuduti et al., 2017;  
92 Feng et al., 2021). Although many acylsugar metabolic genes (AMGs) have been identified in  
93 recent years, several remain unidentified and the regulation of acylsugar biosynthesis has not  
94 been well characterized, especially with regard to how solanaceous trichomes can support  
95 production of high levels of specialized metabolites.

96 *Solanum pennellii*, a wild relative of the cultivated tomato *Solanum lycopersicum*, is  
97 endemic to arid western slopes of the Peruvian Andes and is known for its ability to withstand  
98 extreme drought conditions. Acylsugars secreted from glandular trichomes of *S. pennellii*  
99 represent a remarkably large fraction, up to 20%, of the leaf dry weight; in contrast, *S.*  
100 *lycopersicum* produces only ~1% of its leaf dry weight as acylsugars. (Fobes et al., 1985). Here,  
101 in order to identify AMGs, we first created a *S. lycopersicum* x *S. pennellii* F<sub>2</sub> population and  
102 conducted transcriptomic comparisons between high- and low-acylsugar-producing F<sub>2</sub>  
103 individuals to identify candidate AMGs. Next, we compared this list with our previously  
104 published list of candidate AMGs (Mandal et al., 2020). Additionally, genome-wide  
105 nonsynonymous to synonymous substitution rates (dN/dS ratio) estimation of *S. pennellii* and *S.*  
106 *lycopersicum* putative orthologs refined the list of candidate genes, and analysis of trichome-  
107 preferential expression identified three candidates- *Sopen05g009610*, encoding a beta-ketoacyl-  
108 (acyl-carrier-protein) reductase (*SpKAR1* hereafter; a component of the FAS complex),  
109 *Sopen07g006810*, encoding a small subunit of Rubisco (*SpRBCS1* hereafter), and  
110 *Sopen05g032580*, encoding an induced stolon-tip protein like member (*SpSTPL* hereafter).  
111 Virus-induced gene silencing (VIGS) indicated roles for both *SpKAR1* and *SpRBCS1* in  
112 acylsugar metabolism, while silencing of *SpSTPL* had no effect. The role of *SpRBCS1* was  
113 further supported by  $\delta^{13}\text{C}$  analyses of acylsugars. Additionally, phylogenetic analyses and data

114 mining revealed interesting evolutionary aspects which suggested that orthologs of SpKAR1 and  
115 SpRBCS1 are involved in specialized metabolism in other plants.

## 116 **Results:**

### 117 **Transcriptomic comparison between high- and low-acylsugar-producing F<sub>2</sub> individuals of** 118 ***S. lycopersicum* x *S. pennellii***

119 *S. pennellii* accession LA0716 produces copious amount of acylsugars (~20% of leaf dry  
120 weight), whereas *S. lycopersicum* cv. VF36 accumulates considerably lower amount (~1% of  
121 leaf dry weight) (Fobes et al., 1985). The interspecific F<sub>1</sub> hybrid (LA4135) accumulates low  
122 levels of acylsugars (<3% of leaf dry weight). To identify candidate AMGs, we first analyzed  
123 acylsugar accumulation in an F<sub>2</sub> population derived from the cross between VF36 and LA0716.  
124 Of the 114 F<sub>2</sub> plants, 24 accumulated acylsugars >10% of their leaf dry weight, whereas 62  
125 accumulated acylsugars <3% of their leaf dry weight (Figure 1A). Next, using RNA-seq, we  
126 identified genes that were differentially expressed between 10 high- and 10 low-acylsugar-  
127 producing F<sub>2</sub> individuals (hereafter referred to as HIGH-F<sub>2</sub> and LOW-F<sub>2</sub>, respectively). A total of  
128 20,160 *S. pennellii* genes were selected after minimum-expression-level filtering, and 331  
129 differentially expressed genes (DEGs) were identified; of these, 134 and 197 DEGs showed  
130 higher and lower expression levels, respectively, in the HIGH-F<sub>2</sub> group compared to the LOW-F<sub>2</sub>  
131 group (Supplemental Data Set 1). Enrichment analysis indicated that gene ontology (GO) terms  
132 such as “acyltransferase activity” (GO:0016747), “fatty acid metabolic process” (GO:0006631),  
133 and “active transmembrane transporter activity” (GO:0022804) were over-represented in the list  
134 of 331 DEGs (Supplemental Figure S1).

135 Of the 331 DEGs, 73 were also differentially expressed between high- and low-  
136 acylsugar-producing accessions of *S. pennellii* (Mandal et al., 2020). Many genes with known  
137 and putative roles in acylsugar metabolism showed higher expression levels in the HIGH-F<sub>2</sub>  
138 group compared to the LOW-F<sub>2</sub> group (Figure 1B), which validated our RNA-seq approach.  
139 These genes encode branched-chain fatty acid metabolic proteins, FAS components, acyl-  
140 activating enzymes (also known as acyl-CoA synthetases), a mitochondrial/peroxisomal  
141 membrane protein (Sopen11g007710), three ATP-binding cassette transporters, three ASATs,  
142 transcription factors, and a Rubisco small subunit. Additionally, known and putative flavonoid  
143 metabolic genes, such as *Sopen11g003320* (UDP-glucose:catechin glucosyltransferase) and three

144 sequential genes on chromosome 6 (*Sopen06g034810*, *Sopen06g034820*, and *Sopen06g034830*;  
145 myricetin *O*-methyltransferase; (Kim et al., 2014)), which are strongly co-expressed with AMG  
146 (Mandal et al., 2020), were also found in the list of DEGs (Supplemental Data Set 1).

147

#### 148 **Genome-wide dN/dS ratio estimation of *S. pennellii* and *S. lycopersicum* putative orthologs** 149 **and refinement of candidate AMG list**

150 In addition to difference in gene expression levels, difference in protein-coding sequence may  
151 also contribute to difference in acylsugar accumulation capabilities between *S. pennellii* and *S.*  
152 *lycopersicum*. Compared to primary metabolic genes, specialized metabolic genes evolve faster  
153 and exhibit higher ratio of nonsynonymous to synonymous substitution rates (dN/dS ratio)  
154 (Moore et al., 2019). Therefore, as an additional approach for identifying candidate AMGs, we  
155 performed a genome-wide dN/dS ratio analysis (Yang and Nielsen, 2000) of *S. pennellii* and *S.*  
156 *lycopersicum* putative orthologs to identify genes that are under positive selection. Using  
157 reciprocal BLAST, 19,984 putative ortholog pairs were selected (Supplemental Data Set 2), and  
158 the yn00 maximum-likelihood method (Yang, 1997) yielded a genome-wide mean dN/dS ratio of  
159 0.3273 (Figure 2A). A total of 732 genes with dN/dS >1.0 were considered to be under positive  
160 selection (Supplemental Data Set 3).

161 To narrow our focus further, we next compared lists of candidate AMGs obtained from  
162 three approaches: (A) 331 DEGs identified in our analysis of the F<sub>2</sub> population, (B) 1,087 DEGs  
163 we previously reported from transcriptomic analysis between high- and low-acylsugar-producing  
164 *S. pennellii* accessions (Mandal et al., 2020), and (C) 732 genes with dN/dS >1.0. Four genes  
165 (*Sopen07g006810*, *Sopen05g009610*, *Sopen05g032580*, and *Sopen05g034770*) occurred in all  
166 three sets (Figure 2B, Table 1). Next, we measured trichome-enriched expression of these four  
167 candidates, since many AMGs are expressed in trichome tip-cells (Ning et al., 2015; Schillmiller  
168 et al., 2015; Fan et al., 2016; Fan et al., 2020). Transcript levels of *Sopen07g006810* (*SpRBCS1*),  
169 *Sopen05g009610* (*SpKARI*), and *Sopen05g032580* (*SpSTPL*) were 220-, 110- and 13-fold,  
170 respectively, higher in isolated stem trichomes than in underlying tissues of shaved stems in *S.*  
171 *pennellii* accession LA0716. On the other hand, expression of *Sopen05g034770* was lower in  
172 trichomes than in shaved stems (Figure 2C). Because of this, and the fact that expression of

173 *Sopen05g034770* is inversely correlated with acylsugar amount (Table 1), this gene was not  
174 analyzed further.

175

### 176 ***In vivo* functional validation of candidate AMGs**

177 To determine whether *SpRBCS1*, *SpKAR1* and *SpSTPL* are involved in acylsugar biosynthesis,  
178 these three candidate genes were targeted in *S. pennellii* LA0716 for VIGS using tobacco rattle  
179 virus (TRV)-based silencing vectors (Dong et al., 2007). VIGS resulted in significant  
180 downregulation of target genes (82%, 54%, and 94% reduction in transcript levels for *SpRBCS1*,  
181 *SpKAR1*, and *SpSTPL*, respectively; Supplemental Figure S2, A and B), and leaf surface  
182 metabolites were analyzed by liquid chromatography-mass spectrometry (LC-MS). Compared to  
183 a group of control plants (empty TRV vectors), total acylsugar levels decreased by 23% ( $P <$   
184 0.05) in VIGS-*SpRBCS1* plants (Figure 3, A and B; Supplemental Data Set 4). In contrast, we  
185 did not observe any statistically significant changes in total acylsugar amount upon suppression  
186 of *SpKAR1* or *SpSTPL* (Figure 3A).

187 Despite the lack of influence on total acylsugar amount, silencing of *SpKAR1* led to  
188 significant reductions in acylsugar medium-chain fatty acids (18%, 23%, and 20% reductions for  
189 8-methylnonanoate, *n*-decanoate, and *n*-dodecanoate, respectively), which is consistent with its  
190 predicted role in medium-chain fatty acid biosynthesis (Figure 3C). Silencing of *SpRBCS1*  
191 resulted in 20% reductions in C5 acyl chains (2- and 3-methylbutanoate). No noticeable  
192 morphological differences were observed between control and silenced plants (Supplemental  
193 Figure S2C), which indicates that these effects on acylsugar phenotypes were not indirect  
194 consequences of abnormal plant growth and development caused by VIGS. Transcript  
195 enrichment in trichomes and VIGS results together indicate roles of *SpRBCS1* and *SpKAR1* in  
196 acylsugar metabolism. On the other hand, no statistically significant changes in acyl chain profile  
197 were observed upon silencing of *SpSTPL*.

198

### 199 **Phylogenetic analysis of *SpKAR1***

200 Short-chain dehydrogenases/reductases (SDRs) constitute a large protein superfamily of  
201 NAD(P)(H)-dependent oxidoreductases; members exhibit low levels of sequence identity, but  
202 they share a Rossmann-fold motif for nucleotide binding (Kavanagh et al., 2008). Many SDRs  
203 are involved in biosynthesis of specialized metabolites, such as sesquiterpene zerumbone in  
204 *Zingiber zerumbet* (Okamoto et al., 2011), diterpene momilactone in *Oryza sativa* (Shimura et  
205 al., 2007), monoterpenoids in glandular trichomes of *Artemisia annua* (Polichuk et al., 2010),  
206 monoterpenoid constituents of essential oils in peppermint and spearmint (Ringer et al., 2005),  
207 phenolic monoterpenes in the Lamiaceae (Krause et al., 2021), and steroidal glycoalkaloids and  
208 saponins in *Solanum* species (Sonawane et al., 2018). SpKAR1 (322-aa) belongs to the SDR  
209 family and shares several common motifs, such as the N-terminal cofactor binding motif  
210 TGxxxGxG, a downstream structural motif (C/N)NAG, the active site motif YxxxK, and the  
211 catalytic tetrad N-S-Y-K, with members of the SDR “classical” subfamily (Kavanagh et al.,  
212 2008) (Supplemental Figure S3). However, phylogenetic analysis suggested that SpKAR1 is  
213 closer to *Escherichia* and *Synechocystis* FabG [beta-ketoacyl-(acyl-carrier-protein) reductase]  
214 than other specialized metabolic SDRs mentioned earlier (Figure 4A; Supplemental Figure S4).  
215 Additionally, these plant SDRs are predicted to have a cytosolic location, whereas SpKAR1 is  
216 predicted to be localized to the chloroplast [TargetP  
217 (<https://services.healthtech.dtu.dk/service.php?TargetP-2.0>), WoLF PSORT  
218 (<https://www.genscript.com/wolf-psort.html>), and MultiLoc2 ([https://abi-services.informatik.uni-  
219 tuebingen.de/multiloc2/webloc.cgi](https://abi-services.informatik.uni-tuebingen.de/multiloc2/webloc.cgi))]. Furthermore, cytochrome P450 monooxygenase (CYP)  
220 activities are closely associated with these specialized metabolic SDRs, whereas SpKAR1  
221 activity presumably is not associated with CYP products. These results together indicate that  
222 SpKAR1 is a component of the FAS complex in the chloroplast, and it is phylogenetically distant  
223 from other specialized metabolic SDRs mentioned earlier.

224 *Capsicum annuum* is a solanaceous species that produces capsaicinoid specialized  
225 metabolites, but not acylsugars. Two SDRs from *Capsicum annuum* showed close phylogenetic  
226 relationships with SpKAR1, and we investigated the similarity between capsaicinoid and  
227 acylsugar biosynthetic pathways. In both pathways, valine is converted to 2-methylpropanoyl-  
228 CoA, which is then elongated to C10 acyl molecules via FAS-mediated reactions (Figure 4B).  
229 This suggests a common evolutionary origin for acyl chain elongation steps in both acylsugar  
230 and capsaicinoid biosynthesis.



231 Ning et al. (2015) reported trichome-enriched expression data for *S. lycopersicum* genes,  
232 and Moghe et al. (2017) reported similar data in four additional acylsugar-producing solanaceous  
233 species- *S. nigrum*, *S. quitoense*, *Hyoscyamus niger*, and *Salpiglossis sinuata*. We mined these  
234 publicly available datasets and investigated if *SpKAR1* orthologs exhibit trichome-enriched  
235 expression. Phylogenetic analysis identified two distinct clades, and members of one clade are  
236 preferentially expressed in trichomes (Figure 4C; Supplemental Figures S5 and S6). This  
237 suggests that *SpKAR1* orthologs have a role in trichome acylsugar biosynthesis in other  
238 solanaceous species.

239

#### 240 **Phylogenetic analysis of *SpRBCS1***

241 Rubisco is composed of eight large subunits (encoded by a single *RBCL* gene on the plastid  
242 genome) and eight small subunits (encoded by a multigene family *RBCS* on the nuclear genome).  
243 Among the five annotated *RBCS* genes in *S. pennellii* (three on chromosome 2 and one on each  
244 of chromosome 3 and 7), only *Sopen07g006810* (*SpRBCS1*) exhibited noticeable trichome-  
245 enriched expression based on reverse transcription- quantitative PCR (Supplemental Figure  
246 S7A). In shaved stems, *SpRBCS1* had extremely low, if any, level of expression (if *SpRBCS1* is  
247 trichome-specific, residual expression could be due to incomplete shaving of stem trichomes).  
248 On the other hand, other *RBCS* members showed high expression levels in shaved stems (~1000-  
249 fold higher than *SpRBCS1*). Additionally, protein sequence analysis revealed that other *RBCS*  
250 members, which share >90% sequence identity with each other, share low level of homology  
251 (<55% identity) with *SpRBCS1* (Supplemental Figure S7, A and B). Furthermore,  
252 *Sopen07g006810-Solyc07g017950* ortholog pair had dN/dS ratio of 2.91, whereas ortholog pairs  
253 of other *RBCS* members showed dN/dS ratios less than 0.32 (Supplemental Data Set 3), which is  
254 expected from highly conserved, mesophyll-expressed “regular” *RBCS* members (presumably  
255 involved in primary metabolism). These results indicated that *SpRBCS1* is distinct from other  
256 *RBCS* members. This was supported by phylogenetic analysis, which in conjunction with data  
257 mining, showed that orthologs of *SpRBCS1* are preferentially expressed in trichomes of  
258 solanaceous members (average 112-fold in six species where trichome-enriched expression data  
259 are available; Figure 5; Supplemental Figures S8 and S9). Interestingly, *SpRBCS1* was placed in  
260 a monophyletic clade with *Nicotiana tabacum RBCS-T*, which is expressed in trichome tip cells

261 (Laterre et al., 2017). Orthologs of SpRBCS1 were found outside the Solanaceae (including  
262 *Oryza sativa*), but not in Arabidopsis, which lacks glandular trichomes.

263

### 264 $\delta^{13}\text{C}$ analyses of acylsugars

265 Based on a previous metabolomics study (Balcke et al., 2017), it was hypothesized that Rubisco  
266 in trichomes mainly recycles  $\text{CO}_2$  released by the high metabolic rate in these cells. In *S.*  
267 *pennellii* trichomes, where production of acylsugars is high, three steps in this pathway release  
268  $\text{CO}_2$ : acetolactate synthase, isopropylmalate dehydrogenase, and branched-chain ketoacid  
269 dehydrogenase. If trichome Rubisco is responsible for recycling  $\text{CO}_2$ , then acylsugars (and other  
270 metabolites in trichomes) will contain some carbon that has undergone at least two rounds of  
271 fixation, first in the bulk of the plant to provide primary metabolites, and again in the trichome to  
272 recover  $\text{CO}_2$  released during production of branched chain fatty acids. One consequence of this  
273 re-fixation would be that acylsugars contain even less  $^{13}\text{C}$  than the rest of the plant due to  
274 isotopic fractionation at each fixation (the lighter  $^{12}\text{C}$  isotope would be favored because of a  
275 lower activation energy). To test this hypothesis, we measured fractionation of carbon isotopes  
276 ( $\delta^{13}\text{C}$ ; reported in parts per thousand ‰) in both secreted acylsugars and plant tissues  
277 presumably without acylsugars (shaved stems). Acylsugars and shaved stems showed  $\delta^{13}\text{C}$  of -  
278 33.15‰ and -28.99‰, respectively (Figure 6A). The difference in  $\delta^{13}\text{C}$  between these two  
279 sample types indicates that acylsugars contain carbons that have undergone additional rounds of  
280 fixation compared to non-acylsugar metabolites. Additionally,  $\delta^{13}\text{C}$  values from *S. pennellii*  
281 samples (acylsugars and shaved stems) are comparable to  $\delta^{13}\text{C}$  value from another member of  
282 the Solanaceae that was reported previously (-30.7‰ in *Nicotiana tabacum*) (Smith and Epstein,  
283 1971).

284 Next, we hypothesized that the trichome-preferentially-expressed *SpRBCS1* is  
285 responsible for this re-fixation of carbons into acylsugars. To test our hypothesis, we determined  
286 the difference in  $\delta^{13}\text{C}$  between shaved stems and acylsugars ( $\delta\delta^{13}\text{C}$ ) for two groups of plants-  
287 control and VIGS-*SpRBCS1*. Compared to a control group, VIGS led to a reduction in  $\delta\delta^{13}\text{C}$   
288 (Figure 6B), which confirmed the role of *SpRBCS1* in supplying re-fixed carbons for acylsugar  
289 biosynthesis.

290

## 291 **Discussion**

292 Acylsugars are secreted by glandular trichomes of several plant families, including Martyniaceae  
293 (Asai et al., 2010), Caryophyllaceae (Asai et al., 2012), Geraniaceae (Sakai et al., 2013), and  
294 Solanaceae, where they have been best studied. A detailed knowledge about genes involved in  
295 regulating acylsugar amount and acyl chain profile (Ben-Mahmoud et al., 2018) is required for  
296 successful crop breeding programs and metabolic engineering of acylsugar production. Here, we  
297 report two trichome-preferentially-expressed genes involved in acylsugar biosynthesis.

298

## 299 **Multiple approaches to identify and validate candidate AMGs**

300 Many enzymes involved in acylsugar biosynthesis have been identified in recent years (Ning et  
301 al., 2015; Schillmiller et al., 2015; Fan et al., 2016; Schillmiller et al., 2016; Moghe et al., 2017;  
302 Nadakuduti et al., 2017; Fan et al., 2020; Mandal et al., 2020; Feng et al., 2021; Lou et al., 2021).  
303 To identify additional enzymes in this pathway, and hopefully regulatory proteins, we used a  
304 multipronged strategy to find genes whose expression and evolutionary patterns suggested they  
305 could be involved. To refine our previously reported list of candidate AMGs (Mandal et al.,  
306 2020), we looked for genes that were differentially expressed between high- and low-acylsugar-  
307 producing F<sub>2</sub> individuals derived from *S. lycopersicum* x *S. pennellii*, and also genes that  
308 appeared to be rapidly evolving as determined by the dN/dS ratio. The intersection of three sets  
309 of candidate AMGs yielded four candidates (Figure 2B). One candidate, *Sopen05g034770*, had  
310 lower expression in high-acylsugar-producing F<sub>2</sub> individuals than in low-acylsugar-producing F<sub>2</sub>  
311 individuals and also lower expression in trichomes relative to underlying tissue (Table 1; Figure  
312 2C). Both of these patterns are opposite to what we would expect for genes involved in acylsugar  
313 biosynthesis. Therefore, this gene was not studied further, but the hypothetical protein encoded  
314 by this gene may act as a negative regulator of the pathway. Putative roles of the remaining three  
315 trichome-preferentially-expressed candidates in acylsugar biosynthesis were tested using VIGS,  
316 which confirmed *SpKARI* and *SpRBCS1* as AMGs (Figure 3). Phylogenetic analyses and data  
317 mining revealed that orthologs of both *SpKARI* (Figure 4C) and *SpRBCS1* (Figure 5) are  
318 trichome-preferentially-expressed members in the Solanaceae, suggesting roles for these

319 orthologs in acylsugar biosynthesis. Additionally, *SpKAR1* and *SpRBCS1* exemplify duplication  
320 of highly-conserved primary metabolic genes followed by spatial regulation of gene expression  
321 as a driver of evolution of acylsugar metabolism.

322

### 323 **Function and phylogeny of SpKAR1**

324 In plants, *de novo* fatty acid biosynthesis takes place predominantly in plastids, which use a  
325 multicomponent type II FAS system that catalyzes the extension of the growing acyl chain. The  
326 plastidic FAS has four well-characterized enzymatic components: a beta-ketoacyl-(acyl-carrier-  
327 protein) reductase (KAR), a beta-hydroxyacyl-(acyl-carrier-protein) dehydrase, an enoyl-(acyl-  
328 carrier-protein) reductase, and three isozymes of beta-ketoacyl-(acyl-carrier-protein) synthases  
329 (KAS I, II, and III). KAR catalyzes one of the steps of the core four-reaction cycle of the FAS-  
330 mediated chain elongation process. Close phylogenetic relationship with bacterial FabG (KAR)  
331 and its predicted chloroplast location indicate that SpKAR1 is a component of the plastid FAS,  
332 and it is distinct from other specialized metabolic cytosolic SDRs (Figure 4A). VIGS showed  
333 that SpKAR1 is required for acylsugar straight-chain fatty acid (SCFA) biosynthesis (Figure 3C),  
334 and we previously reported two trichome-preferentially-expressed KAS genes that are involved  
335 in SCFA biosynthesis (Mandal et al., 2020). These results corroborate the role of FAS in  
336 acylsugar SCFA biosynthesis.

337         Elongation of acetyl-CoA to SCFAs by FAS complex presumably takes place in plastids;  
338 however, it is not clear if elongation of 2-methylpropanoyl-CoA (isobutyryl-CoA; produced in  
339 mitochondria from valine) to 8-methylnonanoyl-CoA (one of the major branched-chain acyl  
340 groups) occurs in mitochondria or chloroplast (Figure 4B). For both capsaicinoid (Mazourek et  
341 al., 2009) and acylsugar (Slocombe et al., 2008) biosynthesis, it has been proposed that 2-  
342 methylpropanoyl-CoA is transported from mitochondria to chloroplast, where it is elongated by  
343 the plastid FAS complex. Recently, a dual-localized KAR (AT1G24360) was reported in  
344 Arabidopsis (Guan et al., 2020), and AT1G24360 is phylogenetically closely related to SpKAR1  
345 (Figure 4C; Supplemental Figure S5). This suggests the possibility that plastidic-SpKAR1 is  
346 involved in the biosynthesis of acylsugar SCFAs, whereas mitochondrial-SpKAR1 is involved in  
347 the elongation of 2-methylpropanoyl-CoA; this would allow 2-methylpropanoyl-CoA to be  
348 elongated without being transported to plastid.

349

### 350 **Capsaicinoid and acylsugar biosynthetic pathways**

351 In *Capsicum*, 8-methyl-6-nonenoyl-CoA (C10) and 8-methylnonanoyl-CoA (C10) are attached  
352 to an aromatic compound derived from phenylalanine to generate capsaicin and  
353 dihydrocapsaicin, respectively, which are two of the most potent capsaicinoids (Mazourek et al.,  
354 2009). These C10 acyl molecules are presumably derived from 2-methylpropanoyl-CoA via  
355 FAS-mediated reactions, and this segment of the capsaicinoid biosynthetic pathway is similar to  
356 the acylsugar biosynthetic pathway (Figure 4B). Attachment of acyl groups to an aromatic  
357 compound (in case of capsaicinoid biosynthesis) or sucrose (in case of acylsugar biosynthesis) is  
358 catalyzed by BAHD superfamily transferases: PUN1 in capsaicinoid biosynthesis (Stewart et al.,  
359 2005) and ASATs in acylsugar biosynthesis (Schilmiller et al., 2015; Fan et al., 2016). Moghe et  
360 al. (2017) reported that PUN1 and ASATs share a common evolutionary ancestor, and our  
361 phylogenetic analysis revealed that SpKAR1 is closely related to two reductases involved in  
362 capsaicinoid biosynthesis (FAS-mediated acyl chain elongation steps) (Figure 4A). These results  
363 indicate close phylogenetic relationships between segments of capsaicinoid and acylsugar  
364 biosynthetic pathways. Additionally, acyl chain length is an important factor in determining both  
365 pungency of capsaicinoids and potential in defense activity of acylsugars (Ben-Mahmoud et al.,  
366 2018). Taken together, these findings will be useful in future metabolic engineering of  
367 capsaicinoid and acylsugar production.

368

### 369 **Function and phylogeny of SpRBCS1**

370 Phylogenetic analysis clustered *SpRBCS1* with other solanaceous trichome-preferentially-  
371 expressed *RBCS* members (Figure 5), including *Nicotiana tabacum* tip-cell-expressed *RBCS-T*  
372 (Laterre et al., 2017), and also with rice *OsRBCS1*, which is expressed in several tissues other  
373 than leaf blade (major photosynthetic organ) (Morita et al., 2014). Additionally, based on  
374 enzymatic properties, both *RBCS-T* and *OsRBCS1* were found to be distinct from “regular”  
375 *RBCS* members in respective species. These findings indicate specialized functions for  
376 *SpRBCS1* and its orthologs in special cell/tissue types.

377 Trichome metabolites can accumulate at noticeably high levels; for example, acylsugars  
378 in *S. pennellii* and divatrienediol in *N. tabacum* can accumulate up to 20% and 15%,  
379 respectively, of leaf dry weight (Fobes et al., 1985; Severson et al., 1985). This indicates high  
380 metabolic activities and CO<sub>2</sub> release in trichome cells (for example, enzymatic steps catalyzed by  
381 acetolactate synthase, isopropylmalate dehydrogenase, and branched-chain ketoacid  
382 dehydrogenase complex generate CO<sub>2</sub> during acylsugar production). However, due to thick cell  
383 walls and cuticle, it has been suggested that trichomes have limited gaseous exchange with the  
384 outside and fix little atmospheric CO<sub>2</sub> (Balcke et al., 2017). In order to support continued high  
385 metabolic activities, trichomes may require re-fixation of metabolic CO<sub>2</sub> with a Rubisco that is  
386 active in high CO<sub>2</sub> and low pH conditions. Biochemical assays indicate that *N. tabacum* RBCS-T  
387 has been adapted to such conditions (Laterre et al., 2017). These results encouraged us to  
388 investigate, using  $\delta^{13}\text{C}$  analysis, if SpRBCS1 is involved in re-fixation of metabolic CO<sub>2</sub> into  
389 acylsugars.

390 Fractionation of carbon isotopes during photosynthesis occurs predominantly during the  
391 carboxylation reaction (carbon fixation) catalyzed by Rubisco, and it leads to a preferential  
392 enrichment of one stable isotope over another. Photosynthates contain less of the <sup>13</sup>C than the <sup>12</sup>C  
393 due to kinetic isotope effects- the lighter <sup>12</sup>C isotope is preferentially incorporated into products  
394 because it has a higher energy state (a lower activation energy) (Smith and Epstein, 1971). We  
395 used this information about carbon isotope fractionation to analyze metabolites, and tested the  
396 hypothesis based on Balcke et al. (2017) that in trichomes, Rubisco mostly re-fixes metabolic  
397 CO<sub>2</sub>, which are incorporated into specialized metabolites (predominantly acylsugars in case of *S.*  
398 *pennellii*). Our  $\delta^{13}\text{C}$  examination of acylsugars and shaved stems showed recycling of metabolic  
399 CO<sub>2</sub> into acylsugars (Figure 6A). Additionally, VIGS confirmed that the trichome-preferentially-  
400 expressed *SpRBCS1* is responsible for this re-fixation (Figure 6B). Tomato trichomes receive  
401 carbon mostly from leaf sucrose (Balcke et al., 2017); however, re-fixation of metabolic CO<sub>2</sub>  
402 would allow trichomes to maintain a pH homeostasis and also to improve carbon utilization for  
403 sustained high level production of specialized metabolites.

404

## 405 **Materials and methods**

### 406 **Plant materials and growth conditions**

407 Seeds of *Solanum pennellii* LA0716 and the F<sub>1</sub> hybrid (LA4135) of *S. lycopersicum* VF36 x *S.*  
408 *pennellii* LA0716 were obtained from the C.M. Rick Tomato Genetics Resource Center  
409 (University of California, Davis). The LA4135 was self-pollinated for generating the F<sub>2</sub>  
410 population. Seeds were treated with 1.2% (w/v) sodium hypochlorite for 20 minutes and rinsed  
411 with deionized water three times before placing on moist filter paper in petri dishes. After  
412 germination, seedlings were transferred to soil and grown in a growth chamber (16-hour  
413 photoperiod; 24°C/20°C day/night temperature; 150 μMol m<sup>-2</sup> s<sup>-1</sup> photosynthetically active  
414 radiation; 75% relative humidity).

415

#### 416 **Acylsugar collection from F<sub>2</sub> individuals**

417 Secreted acylsugars were collected from three young leaves of 10-week-old F<sub>2</sub> individuals as  
418 three replicates by dipping them in ethanol for 2-3 seconds. Ethanol was completely removed by  
419 evaporation until dryness in a fume hood. Acylsugar amount was determined as a proportion of  
420 leaf dry weight. Leaf dry weights were measured after drying in a 70°C oven for one week.

421

#### 422 **RNA sequencing (RNA-seq)**

423 10 high-acylsugar-producing F<sub>2</sub> individuals (acylsugar amounts >14% of leaf dry weight) and 10  
424 low-acylsugar-producing F<sub>2</sub> individuals (acylsugar amounts <1% of leaf dry weight) were used  
425 in the HIGH-F<sub>2</sub> versus LOW-F<sub>2</sub> transcriptome comparison. After removing surface metabolites  
426 with ethanol for 2-3 seconds, young leaves were immediately frozen with liquid nitrogen, and  
427 stored at -80°C until further use. Total RNA was isolated from leaves using the RNAqueous  
428 Total RNA Isolation Kit (Thermo Fisher Scientific), and the genomic DNA was removed using  
429 the TURBO DNA-Free Kit (Thermo Fisher Scientific). RNA-seq libraries of polyA<sup>+</sup>-selected  
430 samples were prepared using TruSeq Stranded mRNA Library Preparation Kit LT (Illumina).  
431 After quality control, libraries were sequenced on the HiSeq 4000 (Illumina) 150x150-bp paired-  
432 end sequencing platform according to the manufacturer's specifications at the Texas A&M  
433 Genomics and Bioinformatics Service Center, College Station.

434

## 435 **Differential gene expression analysis**

436 Approximately 31 to 48 million (average 36 million) paired-end reads were generated from  
437 RNA-seq libraries. Sequencing reads were processed using Trimmomatic v0.32 (Bolger et al.,  
438 2014) with the following settings: ILLUMINACLIP:TruSeq3-PE-2.fa:2:30:10, LEADING = 20,  
439 TRAILING = 20, SLIDINGWINDOW = 4:20, MINLEN = 100. Approximately 68% of the  
440 reads in each library passed the trimming filter. The trimmed reads were then mapped to the *S.*  
441 *pennellii* LA0716 genome v2.0 (Bolger et al., 2014) using TopHat2 v2.1.0 (Kim et al., 2013)  
442 with the following parameters: -library-type = fr-firststrand, -mate-inner-dist = 0, -mate-std-dev  
443 = 50, -read-realign-edit-dist = 1000, -read-edit-dist = 2, -read-mismatches = 2, -min-anchor-len  
444 = 8, -splice-mismatches = 0, -min-intron-length = 50, -max-intron-length = 50,000, -max-  
445 insertion-length = 3, -max-deletion-length = 3, -max-multihits = 20, -min-segment-intron = 50, -  
446 max-segment-intron = 50,000, -segment-mismatches = 2, -segment-length = 25. 70-85% of the  
447 trimmed reads were mapped to the *S. pennellii* genome. Aligned reads from TopHat2 were  
448 counted for each gene using HTseq package version 0.6.1 (Anders et al., 2015) with the  
449 following parameters: -f bam, -r name, -s reverse, -m union, -a 20. The count files were used to  
450 identify differentially expressed genes (DEGs) using edgeR version 3.32.1 (Robinson et al.,  
451 2010). Fragments per kilobase per million mapped reads (FPKM) value for each gene in each  
452 sample was called with rpkm command in edgeR program. Genes with more than one count per  
453 million (CPM) in at least two samples were used for differential gene expression analysis. DEGs  
454 were identified when  $P$ , corrected for multiple testing, was less than 0.05 (false discovery rate <  
455 0.05), and fold change was greater than 2.

456

## 457 **Identification of putative orthologs and dN/dS estimation**

458 To identify putative orthologs, we performed an all-versus-all reciprocal BLAST between  
459 annotated genes of *S. pennellii* v2.0 (Bolger et al., 2014) and *S. lycopersicum* ITAG2.3 (Tomato  
460 Genome, 2012) with the following settings: minimum percentage identity = 70, minimum  
461 percentage query coverage = 50. Putative orthologs were aligned with ClustalW, and the  
462 alignment information was converted into codon alignments using PAL2NAL (Suyama et al.,  
463 2006). Genome-wide dN/dS ratios were calculated between putative ortholog pairs using the  
464 yn00 maximum likelihood method in the PAML package (Yang, 1997; Yang and Nielsen, 2000).



465

#### 466 **Determination of trichome-enriched expression**

467 Reverse transcription- quantitative PCR (RT-qPCR) was used to measure trichome-enriched  
468 expression of selected genes in *S. pennellii* LA0716, as described in Mandal et al. (2020). RT-  
469 qPCR primers are given in Supplemental Table S1.

470

#### 471 **Virus-induced gene silencing (VIGS)**

472 VIGS was performed using the tobacco rattle virus (TRV)-based vectors (Dong et al., 2007) in *S.*  
473 *pennellii* LA0716. VIGS constructs were designed using the Solanaceae Genomics Network  
474 VIGS tool (<http://vigs.solgenomics.net/>) and were cloned into the pTRV2-LIC vector, in the  
475 antisense orientation, to target selected genes. *Agrobacterium tumefaciens* strain GV3101  
476 harboring pTRV1, pTRV2 constructs, and empty pTRV2 were grown overnight with 50 mg/mL  
477 kanamycin and 10 mg/mL gentamicin at 28°C. Cultures were centrifuged at 8,000g for 5 min at  
478 4°C, and cells were washed and resuspended in infiltration buffer (10 mM MES pH 5.5, 10 mM  
479 MgCl<sub>2</sub>, and 200 µM of acetosyringone). Cell suspensions were incubated at room temperature  
480 for 3 hours, and different pTRV2 cultures were mixed with equal volumes of pTRV1 cultures to  
481 reach final OD<sub>600</sub> = 1 before infiltration at the first true leaf stage with a needleless syringe.  
482 Plants were grown in a chamber with conditions mentioned earlier for approximately six weeks.  
483 Silencing of target genes were assessed with RT-qPCR using primers that were designed outside  
484 the VIGS-targeted regions. VIGS primers are listed in Supplemental Table S1.

485

#### 486 **Chromatography–mass spectrometry analysis**

487 Secreted acylsugars from control and VIGS plants were quantified with liquid chromatography-  
488 mass spectrometry (LC–MS). Acylsugars on leaf surface were collected from similar-sized  
489 young leaves by submerging them in 10 ml of extraction solvent [acetonitrile:isopropanol:water  
490 (3:3:2, v/v/v) with 0.1% formic acid; 100 µM propyl 4-hydroxybenzoate was used as the internal  
491 standard], followed by gentle mixing for 2 minutes. Extracted samples were analyzed using Q  
492 Exactive Focus coupled with Ultimate 3000 RS LC unit (Thermo Fisher Scientific) and Exactive

493 Series 2.8 SP1/Xcalibur 4.0 software. Acylsugars were separated by injecting 10  $\mu$ L of sample  
494 into Acclaim 120 (2.1 x 150 mm; 3  $\mu$ m) C18 column (Thermo Fisher Scientific) that was housed  
495 at 30°C. 0.1% formic acid was used as eluent A and acetonitrile with 0.1% formic acid was used  
496 as eluent B in the mobile phase. Flow rate was set at 300  $\mu$ L/min with the following gradient: 0–  
497 3 minutes, 40% B; 3-23 minutes, 40-100% B; 23-28 minutes, hold 100% B; 28.1-31 minutes,  
498 hold 40% B. The Q Exactive Focus HESI source was operated in full MS in negative  
499 electrospray ionization (ESI) mode. Other parameters were set as follows: sheath and auxiliary  
500 gas flow rates-35 and 10 arbitrary units, respectively; spray voltage- 3.3 kV; S-Lens RF level- 50  
501 v. The transfer capillary temperature and the auxiliary gas heater temperature were held at 320°C  
502 and 350°C, respectively. Parallel reaction monitoring (PRM) mode was used for targeted  
503 MS/MS of acylsugars. Relative abundances of acylsugars were determined by dividing total peak  
504 areas of all detected acylsugars with peak area of the internal standard and leaf dry weight. Dry  
505 weights of the extracted leaves were measured after one week of drying in a 70°C oven.

506 Acylsugar acyl chain profiles were analyzed with gas chromatography-mass spectrometry  
507 (GC–MS) after performing transesterification reaction, as described in Mandal et al. (2020).

508

## 509 **Phylogenetic analysis**

510 Sequences were obtained from the Solanaceae Genomics Network, GenBank, and the NCBI  
511 website. For *S. nigrum*, *S. quitoense*, *Hyoscyamus niger*, and *Salpiglossis sinuata*, *de novo*  
512 assembled transcriptomes (Moghe et al., 2017) were used to collect sequences, which were  
513 translated in six possible frames (<https://web.expasy.org/translate/>) to obtain protein sequences  
514 with longest open reading frames. MAFFT (Katoh and Standley, 2013) was used for multiple  
515 sequence alignment with BLOSUM62 matrix, gap extend penalty value of 0.123, and gap  
516 opening penalty value of 1.53. ModelFinder (Kalyaanamoorthy et al., 2017) was used to  
517 compare substitution models, and the best model of protein evolution was selected based on  
518 lowest Bayesian Information Criterion scores (LG+I+G4 for Figure 4A, JTT+G4 for  
519 Supplemental Figure S5, and LG+G4 for Figure 5). IQ-TREE 2 (Minh et al., 2020) was used to  
520 construct maximum-likelihood based phylogenetic trees. MEGA X (Kumar et al., 2018) was  
521 used to construct neighbor-joining phylogenetic trees applying Jones-Taylor-Thornton (JTT)

522 model. Uniform rates among sites were used, and pairwise deletion was used for gaps/missing  
523 data. Bootstrap values were obtained from 1000 replicates.

524

### 525 **Stable isotope analysis**

526  $\delta^{13}\text{C}$  analysis was performed at the Texas A&M Stable Isotope Geosciences Facility using  
527 methods described in McDermott et al. (2019).

528

### 529 **Accession numbers**

530 Sequence data from this article can be found in the GenBank data libraries under accession  
531 numbers ON920880 (SpRBCS1; Sopen07g006810), ON920881 (SpRBCS2; Sopen02g014220),  
532 ON920882 (SpRBCS3; Sopen02g030610), ON920883 (SpRBCS4; Sopen02g030630),  
533 ON920884 (SpRBCS5; Sopen03g007000), ON920885 (SpKAR1; Sopen05g009610),  
534 ON920886 (SpKAR2; Sopen06g028190), ON920887 (SpSTPL; Sopen05g032580), and  
535 ON920888 (hypothetical protein; Sopen05g034770). RNA-seq reads used in this study were  
536 submitted to the NCBI Sequence Read Archive under the accession number PRJNA818092  
537 (BioProject ID).

538

### 539 **Supplemental data**

540 **Supplemental Figure S1.** Enrichment analysis of gene ontology (GO) terms associated with 331  
541 differentially expressed genes (DEGs) between high- and low-acylsugar-producing F<sub>2</sub>  
542 individuals.

543 **Supplemental Figure S2.** Virus-induced gene silencing (VIGS) of candidate genes in *Solanum*  
544 *pennellii* LA0716.

545 **Supplemental Figure S3.** Multiple sequence alignment of SpKAR1 (Sopen05g009610) and its  
546 homologs, including specialized metabolic short-chain dehydrogenases/reductases (SDRs).

547 **Supplemental Figure S4.** Maximum-likelihood phylogenetic tree of SpKAR1  
548 (Sopen05g009610) and related short-chain dehydrogenases/reductases (SDRs).

549 **Supplemental Figure S5.** Maximum-likelihood phylogenetic tree of SpKAR1  
550 (Sopen05g009610) and its homologs in the Solanaceae.

551 **Supplemental Figure S6.** Multiple sequence alignment of SpKAR1 (Sopen05g009610) and its  
552 homologs in the Solanaceae.

553 **Supplemental Figure S7.** Analyses of RBCS members in *Solanum pennellii*.

554 **Supplemental Figure S8.** Neighbor-joining tree of SpRBCS1 (Sopen07g006810) and its  
555 homologs.

556 **Supplemental Figure S9.** Multiple sequence alignment of SpRBCS1 (Sopen07g006810) and its  
557 homologs.

558 **Supplemental Table S1.** List of primers used in this study.

559 **Supplemental Data Set 1.** Differentially expressed genes (DEGs) between HIGH-F<sub>2</sub> and LOW-  
560 F<sub>2</sub> groups.

561 **Supplemental Data Set 2.** Reciprocal Best Hits (RBH) between *Solanum pennellii* and *S.*  
562 *lycopersicum* annotated sequences.

563 **Supplemental Data Set 3.** 732 putative ortholog pairs between *Solanum pennellii* and *S.*  
564 *lycopersicum* with dN/dS > 1.

565 **Supplemental Data Set 4.** Acylsugars from *Solanum pennellii*.

566

## 567 **Acknowledgments**

568 We sincerely thank Charlie Johnson and the staff of the Texas A&M Genomics and  
569 Bioinformatics Center for performing Illumina sequencing, Michael Dickens and the staff of the  
570 Texas A&M High Performance Research Computing Platform for providing computational  
571 resources and assistance, and Christopher Maupin of the Texas A&M Stable Isotope  
572 Geosciences Facility for assistance with  $\delta^{13}\text{C}$  analysis.

573

## 574 **Funding**

575 Early stages of this work were funded by a grant 2011-38821-30891 from the US Department of  
576 Agriculture.

577 *Conflict of interest statement.* None declared.

578

## 579 **Author contributions**

580 WJ and SM designed and performed experiments, analyzed data, and wrote the manuscript. YHR  
581 designed and performed chromatography–mass spectrometry analyses, and reviewed the  
582 manuscript. TDM designed experiments, analyzed data, and wrote the manuscript. All authors  
583 read and approved the final manuscript.

584

## 585 **References**

- 586 **Alba JM, Montserrat M, Fernandez-Munoz R** (2009) Resistance to the two-spotted spider mite  
587 (*Tetranychus urticae*) by acylsucroses of wild tomato (*Solanum pimpinellifolium*) trichomes  
588 studied in a recombinant inbred line population. *Exp Appl Acarol* **47**: 35-47
- 589 **Anders S, Pyl PT, Huber W** (2015) HTSeq—a Python framework to work with high-throughput sequencing  
590 data. *Bioinformatics* **31**: 166-169
- 591 **Asai T, Hara N, Fujimoto Y** (2010) Fatty acid derivatives and dammarane triterpenes from the glandular  
592 trichome exudates of *Ibicella lutea* and *Proboscidea louisiana*. *Phytochemistry* **71**: 877-894
- 593 **Asai T, Nakamura Y, Hirayama Y, Ohyama K, Fujimoto Y** (2012) Cyclic glycolipids from glandular  
594 trichome exudates of *Cerastium glomeratum*. *Phytochemistry* **82**: 149-157
- 595 **Balcke GU, Bennewitz S, Bergau N, Athmer B, Henning A, Majovsky P, Jiménez-Gómez JM,**  
596 **Hoehenwarter W, Tissier A** (2017) Multi-omics of tomato glandular trichomes reveals distinct  
597 features of central carbon metabolism supporting high productivity of specialized metabolites.  
598 *Plant Cell* **29**: 960-983
- 599 **Ben-Mahmoud S, Smeda JR, Chappell TM, Stafford-Banks C, Kaplinsky CH, Anderson T, Mutschler MA,**  
600 **Kennedy GG, Ullman DE** (2018) Acylsugar amount and fatty acid profile differentially suppress  
601 oviposition by western flower thrips, *Frankliniella occidentalis*, on tomato and interspecific  
602 hybrid flowers. *PLoS One* **13**: e0201583
- 603 **Bolger A, Scossa F, Bolger ME, Lanz C, Maumus F, Tohge T, Quesneville H, Alseekh S, Sorensen I,**  
604 **Lichtenstein G, Fich EA, Conte M, Keller H, Schneeberger K, Schwacke R, Ofner I, Vrebalov J, Xu**  
605 **Y, Osorio S, Aflitos SA, Schijlen E, Jimenez-Gomez JM, Ryngajllo M, Kimura S, Kumar R, Koenig**  
606 **D, Headland LR, Maloof JN, Sinha N, van Ham RC, Lankhorst RK, Mao L, Vogel A, Arsova B,**  
607 **Panstruga R, Fei Z, Rose JK, Zamir D, Carrari F, Giovannoni JJ, Weigel D, Usadel B, Fernie AR**  
608 (2014) The genome of the stress-tolerant wild tomato species *Solanum pennellii*. *Nat Genet* **46**:  
609 1034-1038
- 610 **Bolger AM, Lohse M, Usadel B** (2014) Trimmomatic: a flexible trimmer for Illumina sequence data.  
611 *Bioinformatics* **30**: 2114-2120

612 **Bonierbale MW, Plaisted RL, Pineda O, Tanksley SD** (1994) QTL analysis of trichome-mediated insect  
613 resistance in potato. *Theor Appl Genet* **87**: 973-987

614 **Dong Y, Burch-Smith TM, Liu Y, Mamillapalli P, Dinesh-Kumar SP** (2007) A ligation-independent cloning  
615 tobacco rattle virus vector for high-throughput virus-induced gene silencing identifies roles for  
616 *NbMADS4-1* and *-2* in floral development. *Plant Physiol* **145**: 1161-1170

617 **Fan P, Miller AM, Schillmiller AL, Liu X, Ofner I, Jones AD, Zamir D, Last RL** (2016) *In vitro* reconstruction  
618 and analysis of evolutionary variation of the tomato acylsucrose metabolic network. *Proc Natl*  
619 *Acad Sci USA* **113**: E239-248

620 **Fan P, Wang P, Lou YR, Leong BJ, Moore BM, Schenck CA, Combs R, Cao P, Brandizzi F, Shiu SH, Last RL**  
621 (2020) Evolution of a plant gene cluster in Solanaceae and emergence of metabolic diversity.  
622 *eLife* **9**: e56717

623 **Feng H, Acosta-Gamboa L, Kruse LH, Tracy JD, Chung SH, Nava Ferreira AR, Shakir S, Xu H, Sunter G,**  
624 **Gore MA, Casteel CL, Moghe GD, Jander G** (2021) Acylsugars protect *Nicotiana benthamiana*  
625 against insect herbivory and desiccation. *Plant Mol Biol* **109**: 505–522

626 **Fobes JF, Mudd JB, Marsden MP** (1985) Epicuticular lipid accumulation on the leaves of *Lycopersicon*  
627 *pennellii* (Corr.) D'Arcy and *Lycopersicon esculentum* Mill. *Plant Physiol* **77**: 567-570

628 **Guan X, Okazaki Y, Zhang R, Saito K, Nikolau BJ** (2020) Dual-localized enzymatic components constitute  
629 the Fatty acid synthase systems in mitochondria and plastids. *Plant Physiol* **183**: 517-529

630 **Kalyaanamoorthy S, Minh BQ, Wong TKF, von Haeseler A, Jermiin LS** (2017) ModelFinder: fast model  
631 selection for accurate phylogenetic estimates. *Nat Methods* **14**: 587-589

632 **Katoh K, Standley DM** (2013) MAFFT multiple sequence alignment software version 7: improvements in  
633 performance and usability. *Mol Biol Evol* **30**: 772-780

634 **Kavanagh KL, Jornvall H, Persson B, Oppermann U** (2008) Medium- and short-chain  
635 dehydrogenase/reductase gene and protein families : the SDR superfamily: functional and  
636 structural diversity within a family of metabolic and regulatory enzymes. *Cell Mol Life Sci* **65**:  
637 3895-3906

638 **Kim D, Pertea G, Trapnell C, Pimentel H, Kelley R, Salzberg SL** (2013) TopHat2: accurate alignment of  
639 transcriptomes in the presence of insertions, deletions and gene fusions. *Genome Biol* **14**

640 **Kim J, Matsuba Y, Ning J, Schillmiller AL, Hammar D, Jones AD, Pichersky E, Last RL** (2014) Analysis of  
641 natural and induced variation in tomato glandular trichome flavonoids identifies a gene not  
642 present in the reference genome. *Plant Cell* **26**: 3272-3285

643 **Krause ST, Liao P, Crocoll C, Boachon B, Forster C, Leidecker F, Wiese N, Zhao D, Wood JC, Buell CR,**  
644 **Gershenson J, Dudareva N, Degenhardt J** (2021) The biosynthesis of thymol, carvacrol, and  
645 thymohydroquinone in Lamiaceae proceeds via cytochrome P450s and a short-chain  
646 dehydrogenase. *Proc Natl Acad Sci USA* **118**

647 **Kroumova AB, Wagner GJ** (2003) Different elongation pathways in the biosynthesis of acyl groups of  
648 trichome exudate sugar esters from various solanaceous plants. *Planta* **216**: 1013-1021

649 **Kroumova AB, Zaitlin D, Wagner GJ** (2016) Natural variability in acyl moieties of sugar esters produced  
650 by certain tobacco and other Solanaceae species. *Phytochem* **130**: 218-227

651 **Kumar S, Stecher G, Li M, Knyaz C, Tamura K** (2018) MEGA X: Molecular evolutionary genetics analysis  
652 across computing platforms. *Mol Biol Evol* **35**: 1547-1549

653 **Laterre R, Pottier M, Remacle C, Boutry M** (2017) Photosynthetic trichomes contain a specific Rubisco  
654 with a modified pH-dependent activity. *Plant Physiol* **173**: 2110-2120

655 **Lawson DM, Lunde CF, Mutschler MA** (1997) Marker-assisted transfer of acylsugar-mediated pest  
656 resistance from the wild tomato, *Lycopersicon pennellii*, to the cultivated tomato, *Lycopersicon*  
657 *esculentum*. *Mol Breeding* **3**: 307-317

658 **Leckie BM, D'Ambrosio DA, Chappell TM, Halitschke R, De Jong DM, Kessler A, Kennedy GG, Mutschler**  
659 **MA** (2016) Differential and synergistic functionality of acylsugars in suppressing oviposition by  
660 insect herbivores. *PLoS One* **11**: e0153345

661 **Leckie BM, De Jong DM, Mutschler MA** (2012) Quantitative trait loci increasing acylsugars in tomato  
662 breeding lines and their impacts on silverleaf whiteflies. *Mol Breeding* **30**: 1621-1634

663 **Lou YR, Anthony TM, Fiesel PD, Arking RE, Christensen EM, Jones AD, Last RL** (2021) It happened again:  
664 Convergent evolution of acylglucose specialized metabolism in black nightshade and wild  
665 tomato. *Sci Adv* **7**: eabj8726

666 **Luu VT, Weinhold A, Ullah C, Dressel S, Schoettner M, Gase K, Gaquerel E, Xu S, Baldwin IT** (2017) *O*-  
667 acyl sugars protect a wild tobacco from both native fungal pathogens and a specialist herbivore.  
668 *Plant Physiol* **174**: 370-386

669 **Mandal S, Ji W, McKnight TD** (2020) Candidate gene networks for acylsugar metabolism and plant  
670 defense in wild tomato *Solanum pennellii*. *Plant Cell* **32**: 81-99

671 **Mazourek M, Pujar A, Borovsky Y, Paran I, Mueller L, Jahn MM** (2009) A dynamic interface for  
672 capsaicinoid systems biology. *Plant Physiol* **150**: 1806-1821

673 **McDermott EG, Mullens BA, Mayo CE, Roark EB, Maupin CR, Gerry AC, Hamer GL** (2019) Laboratory  
674 evaluation of stable isotope labeling of Culicoides (Diptera: Ceratopogonidae) for adult dispersal  
675 studies. *Parasit Vectors* **12**: 411

676 **Minh BQ, Schmidt HA, Chernomor O, Schrempf D, Woodhams MD, von Haeseler A, Lanfear R** (2020)  
677 IQ-TREE 2: New models and efficient methods for phylogenetic inference in the genomic era.  
678 *Mol Biol Evol* **37**: 1530-1534

679 **Moghe GD, Last RL** (2015) Something old, something new: Conserved enzymes and the evolution of  
680 novelty in plant specialized metabolism. *Plant Physiol* **169**: 1512-1523

681 **Moghe GD, Leong BJ, Hurney SM, Daniel Jones A, Last RL** (2017) Evolutionary routes to biochemical  
682 innovation revealed by integrative analysis of a plant-defense related specialized metabolic  
683 pathway. *eLife* **6**: e28468

684 **Moore BM, Wang P, Fan P, Leong B, Schenck CA, Lloyd JP, Lehti-Shiu MD, Last RL, Pichersky E, Shiu SH**  
685 (2019) Robust predictions of specialized metabolism genes through machine learning. *Proc Natl*  
686 *Acad Sci USA* **116**: 2344-2353

687 **Morita K, Hatanaka T, Misoo S, Fukayama H** (2014) Unusual small subunit that is not expressed in  
688 photosynthetic cells alters the catalytic properties of Rubisco in rice. *Plant Physiol* **164**: 69-79

689 **Nadakuduti SS, Uebler JB, Liu X, Jones AD, Barry CS** (2017) Characterization of trichome-expressed  
690 BAHD acyltransferases in *Petunia axillaris* reveals distinct acylsugar assembly mechanisms within  
691 the Solanaceae. *Plant Physiol* **175**: 36-50

692 **Ning J, Moghe GD, Leong B, Kim J, Ofner I, Wang Z, Adams C, Jones AD, Zamir D, Last RL** (2015) A  
693 feedback-insensitive isopropylmalate synthase affects acylsugar composition in cultivated and  
694 wild tomato. *Plant Physiol* **169**: 1821-1835

695 **Okamoto S, Yu F, Harada H, Okajima T, Hattan J, Misawa N, Utsumi R** (2011) A short-chain  
696 dehydrogenase involved in terpene metabolism from *Zingiber zerumbet*. *FEBS J* **278**: 2892-2900

697 **Polichuk DR, Zhang Y, Reed DW, Schmidt JF, Covello PS** (2010) A glandular trichome-specific  
698 monoterpene alcohol dehydrogenase from *Artemisia annua*. *Phytochemistry* **71**: 1264-1269

699 **Ringer KL, Davis EM, Croteau R** (2005) Monoterpene metabolism. Cloning, expression, and  
700 characterization of (-)-isopiperitenol/(-)-carveol dehydrogenase of peppermint and spearmint.  
701 *Plant Physiol* **137**: 863-872

702 **Robinson MD, McCarthy DJ, Smyth GK** (2010) edgeR: a Bioconductor package for differential expression  
703 analysis of digital gene expression data. *Bioinformatics* **26**: 139-140

- 704 **Sakai T, Tanemura Y, Itoh S, Fujimoto Y** (2013) Dodecyl alpha-L-rhamnopyranosyl-(1-->2)-beta-D-  
705 fucopyranoside derivatives from the glandular trichome exudate of *Erodium pelargoniflorum*.  
706 Chem Biodivers **10**: 1099-1108
- 707 **Schilmiller AL, Gilgallon K, Ghosh B, Jones AD, Last RL** (2016) Acylsugar acylhydrolases:  
708 Carboxylesterase-catalyzed hydrolysis of acylsugars in tomato trichomes. Plant Physiol **170**:  
709 1331-1344
- 710 **Schilmiller AL, Moghe GD, Fan P, Ghosh B, Ning J, Jones AD, Last RL** (2015) Functionally divergent  
711 alleles and duplicated loci encoding an acyltransferase contribute to acylsugar metabolite  
712 diversity in *Solanum* trichomes. Plant Cell **27**: 1002-1017
- 713 **Severson RF, Johnson AW, Jackson DM** (1985) Cuticular constituents of tobacco: factors affecting their  
714 production and their role in insect and disease resistance and smoke quality. Recent Advances in  
715 Tobacco Science **11**: 105–173
- 716 **Shimura K, Okada A, Okada K, Jikumaru Y, Ko KW, Toyomasu T, Sassa T, Hasegawa M, Kodama O,**  
717 **Shibuya N, Koga J, Nojiri H, Yamane H** (2007) Identification of a biosynthetic gene cluster in rice  
718 for momilactones. J Biol Chem **282**: 34013-34018
- 719 **Slocombe SP, Schauvinhold I, McQuinn RP, Besser K, Welsby NA, Harper A, Aziz N, Li Y, Larson TR,**  
720 **Giovannoni J, Dixon RA, Broun P** (2008) Transcriptomic and reverse genetic analyses of  
721 branched-chain fatty acid and acyl sugar production in *Solanum pennellii* and *Nicotiana*  
722 *benthamiana*. Plant Physiol **148**: 1830-1846
- 723 **Smith BN, Epstein S** (1971) Two categories of c/c ratios for higher plants. Plant Physiol **47**: 380-384
- 724 **Sonawane PD, Heinig U, Panda S, Gilboa NS, Yona M, Kumar SP, Alkan N, Unger T, Bocobza S, Pliner M,**  
725 **Malitsky S, Tkachev M, Meir S, Rogachev I, Aharoni A** (2018) Short-chain  
726 dehydrogenase/reductase governs steroidal specialized metabolites structural diversity and  
727 toxicity in the genus *Solanum*. Proc Natl Acad Sci USA **115**: E5419-E5428
- 728 **Stewart C, Jr., Kang BC, Liu K, Mazourek M, Moore SL, Yoo EY, Kim BD, Paran I, Jahn MM** (2005) The  
729 PUN1 gene for pungency in pepper encodes a putative acyltransferase. Plant J **42**: 675-688
- 730 **Suyama M, Torrents D, Bork P** (2006) PAL2NAL: robust conversion of protein sequence alignments into  
731 the corresponding codon alignments. Nucleic Acids Res **34**: W609-612
- 732 **Tomato Genome C** (2012) The tomato genome sequence provides insights into fleshy fruit evolution.  
733 Nature **485**: 635-641
- 734 **Walters DS, Steffens JC** (1990) Branched chain amino acid metabolism in the biosynthesis of  
735 *Lycopersicon pennellii* glucose esters. Plant Physiol **93**: 1544-1551
- 736 **Weinhold A, Baldwin IT** (2011) Trichome-derived O-acyl sugars are a first meal for caterpillars that tags  
737 them for predation. Proc Natl Acad Sci USA **108**: 7855-7859
- 738 **Yang Z** (1997) PAML: a program package for phylogenetic analysis by maximum likelihood. Comput Appl  
739 Biosci **13**: 555-556
- 740 **Yang Z, Nielsen R** (2000) Estimating synonymous and nonsynonymous substitution rates under realistic  
741 evolutionary models. Mol Biol Evol **17**: 32-43

742

## 743 Tables

744 **Table1.** Four genes identified at the intersections of three sets of candidate AMGs



Gene ID	High vs. Low accessions log <sub>2</sub> FC	HIGH-F <sub>2</sub> vs. LOW-F <sub>2</sub> log <sub>2</sub> FC	dN/dS value	dN/dS rank	Annotation
Sopen07g006810	5.01	1.85	2.91	29	Rubisco small subunit
Sopen05g009610	3.32	1.15	2.8	35	Beta-ketoacyl-(acyl-carrier-protein) reductase
Sopen05g032580	2.97	2.1	1.52	227	Induced stolon tip protein-like
Sopen05g034770	-3.48	-1.89	1.59	199	Uncharacterized protein

745  
746 Log<sub>2</sub>FC indicates log<sub>2</sub> (fold-change). Positive and negative log<sub>2</sub>FC values indicate higher and  
747 lower expression levels, respectively, in high-acylsugar-producing *S. pennellii* accessions  
748 (Mandal et al., 2020) or HIGH-F<sub>2</sub> group. dN/dS rank represents the corresponding rank of  
749 selected gene in 732 putative orthologs with dN/dS > 1.

750  
751 **Figure legends**

752  
753 **Figure 1** Acylsugar accumulation and expression of known and candidate acylsugar metabolic  
754 genes (AMGs) in a *Solanum lycopersicum* VF36 x *S. pennellii* LA0716 F<sub>2</sub> population. A,  
755 Histogram showing acylsugar amount distribution among 114 F<sub>2</sub> plants. For each plant, three  
756 replicates were used to measure acylsugar amount. B, Heatmap showing relative expression  
757 levels (set to one-fold in the LOW-F<sub>2</sub> group) of genes with known and putative roles in acylsugar  
758 metabolism. *S. pennellii* gene identifier numbers (Sopen IDs) are given with annotations.  
759 BCAA= branched-chain amino acid; BCFA= branched-chain fatty acid; FAS= fatty acid  
760 synthase component; AAE= acyl-activating enzyme; ASAT= acylsugar acyltransferase; ASH=  
761 acylsugar acylhydrolase; TF= transcription factor; BCKDH= branched-chain keto acid  
762 dehydrogenase; AACs1= acylsugar acyl-CoA synthetase 1; AECH1= acylsugar enoyl-CoA  
763 hydratase 1; ASFF1= acylsucrose fructofuranosidase 1.

764  
765 **Figure 2** Selection of candidate AMGs. A, Distribution of nonsynonymous to synonymous  
766 substitution rate ratios (dN/dS ratios) of putative ortholog pairs from *S. pennellii* and *S.*  
767 *lycopersicum*. B, Venn diagram showing the intersections of three sets of candidate AMGs: (1)  
768 differentially expressed genes (DEGs) between high- and low-acylsugar-producing *S. pennellii*  
769 accessions (Mandal et al., 2020; red circle), (2) DEGs between high- and low-acylsugar-  
770 producing F<sub>2</sub> plants (HIGH-F<sub>2</sub> and LOW-F<sub>2</sub>, respectively; purple circle), and (3) genes with

771 dN/dS > 1 between *S. pennellii* and *S. lycopersicum* putative orthologs (green circle). Four genes  
772 were identified at the intersections of these three sets. C, Relative expression levels of the four  
773 candidate AMGs [*SpRBCS1* (*Sopen07g006810*), *SpKAR1* (*Sopen05g009610*), *SpSTPL*  
774 (*Sopen05g032580*) and *Sopen05g034770*] in isolated stem trichomes and underlying tissues of  
775 shaved stems (normalized to one-fold) in *S. pennellii* LA0716. *SpASAT1* (*Sopen12g002290*), the  
776 ortholog of *S. lycopersicum* trichome tip-cell-expressed *ASAT1* (Fan et al., 2016), was included  
777 for comparison. Error bars indicate SE ( $n = 5$  individual plants).

778  
779 **Figure 3** Virus-induced gene silencing (VIGS) of three trichome-preferentially-expressed  
780 candidate AMGs in *S. pennellii* LA0716. A, Acylsugar quantification by liquid chromatography–  
781 mass spectrometry (LC-MS). To quantify acylsugar amounts, chromatogram peak areas were  
782 normalized by internal standard (IS) area and leaf dry weight (LDW). Error bars indicate SE ( $n =$   
783 10, 12, 11, and 12 individual plants for control, VIGS-*KAR1*, VIGS-*RBCS1* and VIGS-*STPL*  
784 groups, respectively; \*  $P < 0.05$ ; Dunnett's test). B, Representative chromatograms (normalized  
785 by IS area and LDW) showing acylsugar peaks in control and VIGS-*RBCS1* plants. Acylsugar  
786 peaks are listed in Supplemental Data Set 4. C, Acylsugar acyl chain composition analysis by gas  
787 chromatography-mass spectrometry (GC-MS). Predominant acyl chains are shown. Me= methyl;  
788 C3-C12 indicate acyl chain length (for example, 2-MeC3 and *n*-C10 indicate 2-methylpropanoate  
789 and *n*-decanoate, respectively). Error bars indicate SE ( $n = 10, 12, 11,$  and 12 individual plants  
790 for control, VIGS-*KAR1*, VIGS-*RBCS1* and VIGS-*STPL* groups, respectively; \*  $P < 0.05$ , \*\*  $P <$   
791 0.01, \*\*\*  $P < 0.001$ ; Dunnett's test).

792  
793 **Figure 4** Phylogenetic analyses of SpKAR1. A, Maximum-likelihood tree (topology) of  
794 SpKAR1 (*Sopen05g009610*; highlighted) and related short-chain dehydrogenases/reductases  
795 (SDRs). Red circles indicate plant specialized metabolic SDRs. Blue squares indicate bacterial  
796 sequences. "Sopen" numbers indicate sequences from *Solanum pennellii*. Sequences from other  
797 species are given with GenBank accession numbers. Black diamonds indicate more than one  
798 "Sopen" sequences, which were clustered to save space; complete tree is given in Supplemental  
799 Figure S4. Two sequences related to capsaicinoid biosynthesis are indicated by arrows. Bootstrap  
800 values from 1000 replicates are shown on the nodes. B, Similarity between capsaicinoid and  
801 acylsugar biosynthetic pathways. Metabolism of leucine, isoleucine, and straight-chain fatty

802 acids in acylsugar pathway are not shown here. Single arrows do not necessarily indicate single  
803 enzymatic steps. Enzymes are in red font. BCAT= branched-chain aminotransferase; BCKDH=  
804 branched-chain keto acid dehydrogenase; FAS= fatty acid synthase; PUN1= pungent gene 1;  
805 ASAT1= acylsugar acyltransferase 1. C, Neighbor-joining tree of SpKAR1 (highlighted) and its  
806 homologs in the Solanaceae. Sequences from four non-solanaceous plant species [*Ipomoea*  
807 *triloba* and *I. nil* (Convolvulaceae); *Arabidopsis thaliana* and *Brassica napus* (Brassicaceae)]  
808 and two bacteria (*Synechocystis* and *Escherichia*) are also included. Bootstrap values from 1000  
809 replicates are shown. Tree is drawn to scale, with branch lengths measured in the number of  
810 substitutions per site. Tri110x indicates 110-fold higher expression in isolated trichomes  
811 compared to underlying tissues (NF= not found in HN\_c64839g1). RT-qPCR was used for  
812 "Sopen" sequences. Trichome-enriched expression data (based on RNA-seq) for sequences in  
813 five other species were obtained from Ning et al., 2015 (Solyc= *S. lycopersicum*) and Moghe et  
814 al., 2017 (SN= *S. nigrum*; SQ= *S. quitoense*; HN= *Hyoscyamus niger*; SS= *Salpiglossis sinuata*).  
815 Peaxi= *Petunia axillaris*. Sopen03g030230 (138-aa) and its putative orthologs were not included  
816 because they have long deletions and insertions. Maximum-likelihood tree is given in  
817 Supplemental Figure S5.

818

819 **Figure 5** Phylogenetic analysis of SpRBCS1 (Sopen07g006810; highlighted). A, Maximum-  
820 likelihood tree of Rubisco small subunits. Solanaceous sequences were combined into two  
821 clusters (indicated by a red circle and a blue square) to save space. Neighbor-joining tree is given  
822 in Supplemental Figure S8. Bootstrap values from 1000 replicates are shown on the nodes. Tree  
823 is drawn to scale, with branch lengths measured in the number of substitutions per site. Os=  
824 *Oryza sativa*; AT= *Arabidopsis thaliana*. GenBank accession numbers are indicated for *Ipomoea*  
825 *triloba* and *Microcystis aeruginosa*. B and C, Expanded Solanaceae "trichome" cluster (B) and  
826 expanded Solanaceae "regular" cluster (C). Tri220x indicates 220-fold higher expression in  
827 isolated trichomes compared to underlying tissues (NF= not found). RT-qPCR was used for  
828 *Solanum pennellii* (Sopen) sequences. Trichome-enriched expression data (based on RNA-seq)  
829 for sequences in five other species were obtained from Ning et al., 2015 (Solyc= *S.*  
830 *lycopersicum*) and Moghe et al., 2017 (SN= *S. nigrum*; SQ= *S. quitoense*; HN= *Hyoscyamus*  
831 *niger*; SS= *Salpiglossis sinuata*). Peaxi= *Petunia axillaris*; CA= *Capsicum annuum*; Nt=  
832 *Nicotiana tabacum*.

833

834 **Figure 6**  $\delta^{13}\text{C}$  analyses. A, Difference in  $\delta^{13}\text{C}$  values between shaved stems and secreted  
835 acylsugars. Error bars indicate SE ( $n = 10$  individual plants; \*\*\*\*  $P < 0.0001$ ; Welch  $t$ -test). B,  
836 VIGS of *SpRBCSI* reduces the difference in  $\delta^{13}\text{C}$  values between shaved stems and acylsugars.  
837 Error bars indicate SE ( $n = 5$  and  $10$  individual plants for control and VIGS-*RBCSI* groups,  
838 respectively; \*\*\*  $P < 0.001$ ; Welch  $t$ -test).

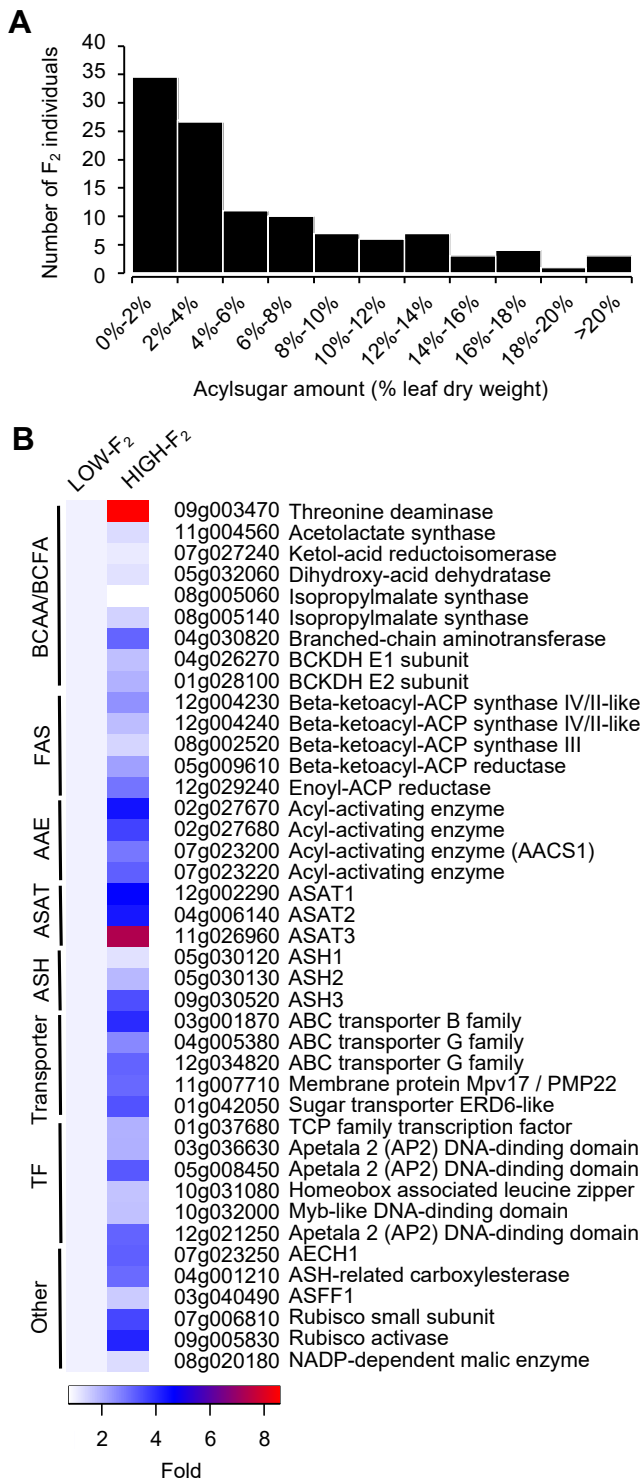


**Figure 1** Acylsugar accumulation and expression of known and candidate acylsugar metabolic genes (AMGs) in a *Solanum lycopersicum* VF36 x *S. pennellii* LA0716 F<sub>2</sub> population. A, Histogram showing acylsugar amount distribution among 114 F<sub>2</sub> plants. For each plant, three replicates were used to measure acylsugar amount. B, Heatmap showing relative expression levels (set to one-fold in the LOW-F<sub>2</sub> group) of genes with known and putative roles in acylsugar metabolism. *S. pennellii* gene identifier numbers (Sopen IDs) are given with annotations. BCAA= branched-chain amino acid; BCFA= branched-chain fatty acid; FAS= fatty acid synthase component; AAE= acyl-activating enzyme; ASAT= acylsugar acyltransferase; ASH= acylsugar acylhydrolase; TF= transcription factor; BCKDH= branched-chain keto acid dehydrogenase; AACS1= acylsugar acyl-CoA synthetase 1; AECH1= acylsugar enoyl-CoA hydratase 1; ASFF1= acylsucrose fructofuranosidase 1.

For reviewers: Please note that the heatmap scale may not be properly displayed on some Macintosh systems.

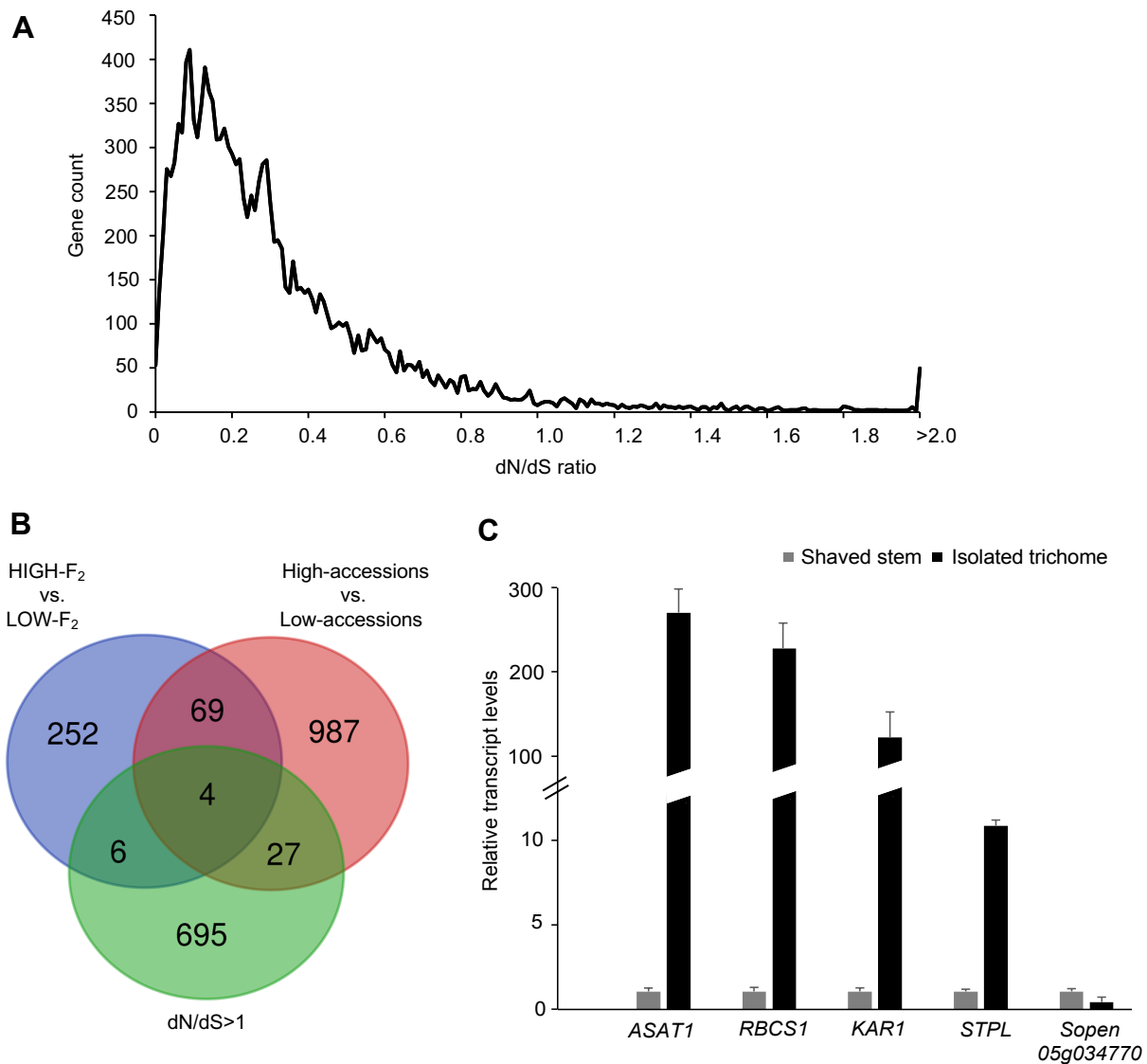


**Figure 2** Selection of candidate AMGs. A, Distribution of nonsynonymous to synonymous substitution rate ratios (dN/dS ratios) of putative ortholog pairs from *S. pennellii* and *S. lycopersicum*. B, Venn diagram showing the intersections of three sets of candidate AMGs: (1) differentially expressed genes (DEGs) between high- and low-acylsugar-producing *S. pennellii* accessions (Mandal et al., 2020; red circle), (2) DEGs between high- and low-acylsugar-producing F<sub>2</sub> plants (HIGH-F<sub>2</sub> and LOW-F<sub>2</sub>, respectively; purple circle), and (3) genes with dN/dS > 1 between *S. pennellii* and *S. lycopersicum* putative orthologs (green circle). Four genes were identified at the intersections of these three sets. C, Relative expression levels of the four candidate AMGs [*SpRBCS1* (*Sopen07g006810*), *SpKAR1* (*Sopen05g009610*), *SpSTPL* (*Sopen05g032580*) and *Sopen05g034770*] in isolated stem trichomes and underlying tissues of shaved stems (normalized to one-fold) in *S. pennellii* LA0716. *SpASAT1* (*Sopen12g002290*), the ortholog of *S. lycopersicum* trichome tip-cell-expressed *ASAT1* (Fan et al., 2016), was included for comparison. Error bars indicate SE ( $n = 5$  individual plants).

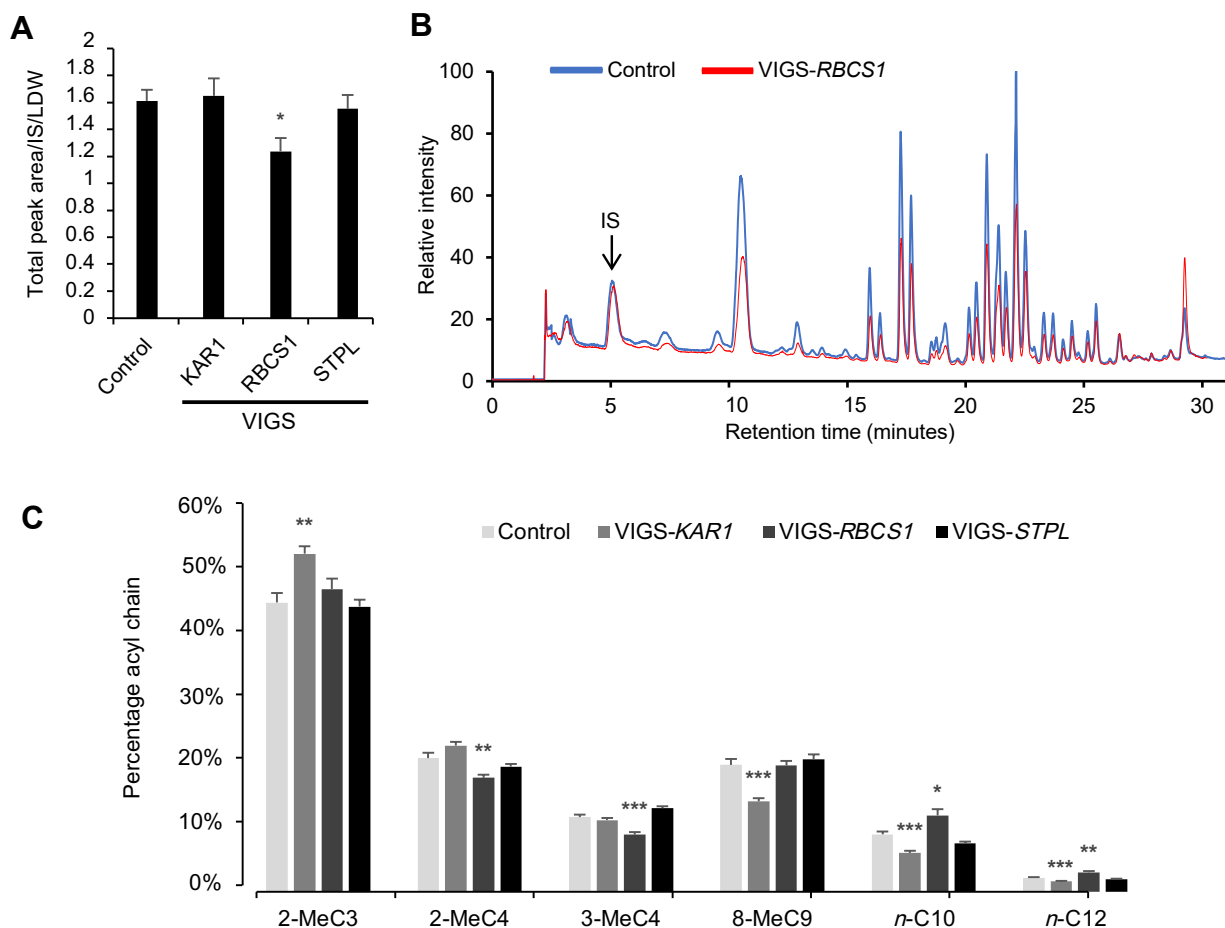


**Figure 3** Virus-induced gene silencing (VIGS) of three trichome-preferentially-expressed candidate AMGs in *S. pennellii* LA0716. A, Acylsugar quantification by liquid chromatography–mass spectrometry (LC-MS). To quantify acylsugar amounts, chromatogram peak areas were normalized by internal standard (IS) area and leaf dry weight (LDW). Error bars indicate SE ( $n = 10, 12, 11,$  and  $12$  individual plants for control, VIGS-KAR1, VIGS-RBCS1 and VIGS-STPL groups, respectively; \*  $P < 0.05$ ; Dunnett’s test). B, Representative chromatograms (normalized by IS area and LDW) showing acylsugar peaks in control and VIGS-RBCS1 plants. Acylsugar peaks are listed in Supplemental Data Set 4. C, Acylsugar acyl chain composition analysis by gas chromatography–mass spectrometry (GC-MS). Predominant acyl chains are shown. Me= methyl; C3-C12 indicate acyl chain length (for example, 2-MeC3 and *n*-C10 indicate 2-methylpropanoate and *n*-decanoate, respectively). Error bars indicate SE ( $n = 10, 12, 11,$  and  $12$  individual plants for control, VIGS-KAR1, VIGS-RBCS1, and VIGS-STPL groups, respectively; \*  $P < 0.05$ , \*\*  $P < 0.01$ , \*\*\*  $P < 0.001$ ; Dunnett’s test).

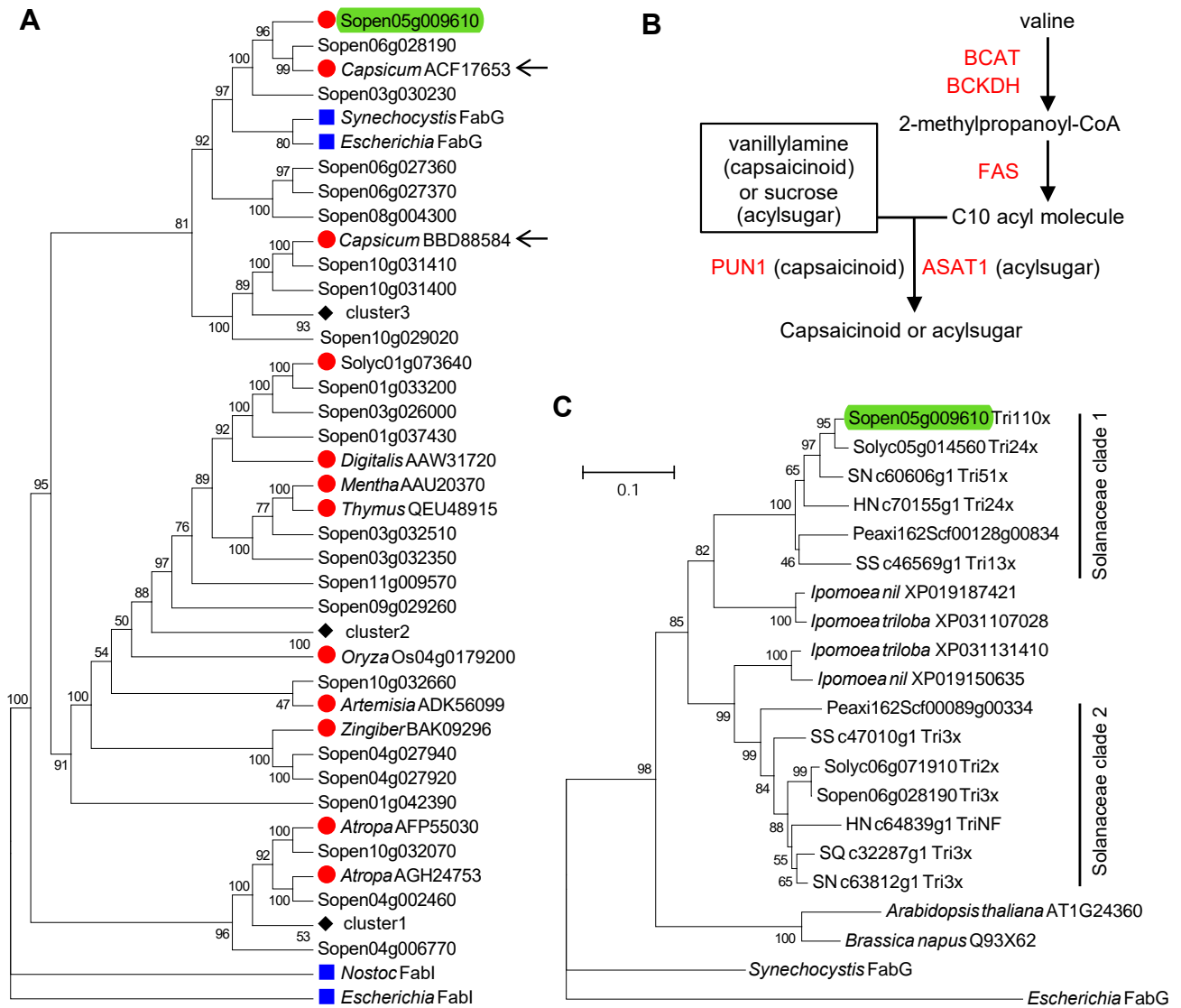


**Figure 4** Phylogenetic analyses of SpKAR1. A, Maximum-likelihood tree (topology) of SpKAR1 (Sopen05g009610; highlighted) and related short-chain dehydrogenases/reductases (SDRs). Red circles indicate plant specialized metabolic SDRs. Blue squares indicate bacterial sequences. "Sopen" numbers indicate sequences from *Solanum pennellii*. Sequences from other species are given with GenBank accession numbers. Black diamonds indicate more than one "Sopen" sequences, which were clustered to save space; complete tree is given in Supplemental Figure S4. Two sequences related to capsaicinoid biosynthesis are indicated by arrows. Bootstrap values from 1000 replicates are shown on the nodes. B, Similarity between capsaicinoid and acylsugar biosynthetic pathways. Metabolism of leucine, isoleucine, and straight-chain fatty acids in acylsugar pathway are not shown here. Single arrows do not necessarily indicate single enzymatic steps. Enzymes are in red font. BCAT= branched-chain aminotransferase; BCKDH= branched-chain keto acid dehydrogenase; FAS= fatty acid synthase; PUN1= pungent gene 1; ASAT1= acylsugar acyltransferase 1. C, Neighbor-joining tree of SpKAR1 (highlighted) and its homologs in the Solanaceae. Sequences from four non-solanaceous plant species [*Ipomoea triloba* and *I. nil* (Convolvulaceae); *Arabidopsis thaliana* and *Brassica napus* (Brassicaceae)] and two bacteria (*Synechocystis* and *Escherichia*) are also included. Bootstrap values from 1000 replicates are shown. Tree is drawn to scale, with branch lengths measured in the number of substitutions per site. Tri110x indicates 110-fold higher expression in isolated trichomes compared to underlying tissues (NF= not found in HN\_c64839g1). RT-qPCR was used for "Sopen" sequences. Trichome-enriched expression data (based on RNA-seq) for sequences in five other species were obtained from Ning et al., 2015 (Solyc= *S. lycopersicum*) and Moghe et al., 2017 (SN= *S. nigrum*; SQ= *S. quitoense*; HN= *Hyoscyamus niger*; SS= *Salpiglossis sinuata*). Peaxi= *Petunia axillaris*. Sopen03g030230 (138-aa) and its putative orthologs were not included because they have long deletions and insertions. Maximum-likelihood tree is given in Supplemental Figure S5.



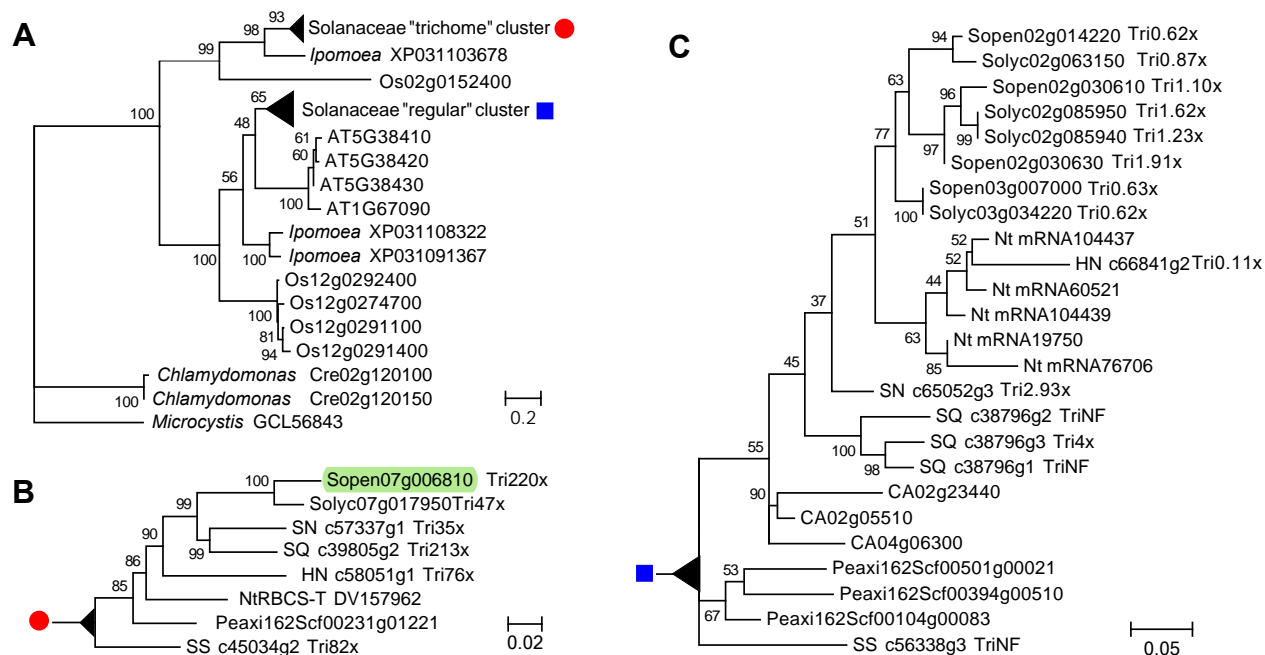


**Figure 5** Phylogenetic analysis of SpRBCS1 (Sopen07g006810; highlighted). A, Maximum-likelihood tree of Rubisco small subunits. Solanaceous sequences were combined into two clusters (indicated by a red circle and a blue square) to save space. Neighbor-joining tree is given in Supplemental Figure S8. Bootstrap values from 1000 replicates are shown on the nodes. Tree is drawn to scale, with branch lengths measured in the number of substitutions per site. Os= *Oryza sativa*; AT= *Arabidopsis thaliana*. GenBank accession numbers are indicated for *Ipomoea triloba* and *Microcystis aeruginosa*. B and C, Expanded Solanaceae "trichome" cluster (B) and expanded Solanaceae "regular" cluster (C). Tri220x indicates 220-fold higher expression in isolated trichomes compared to underlying tissues (NF= not found). RT-qPCR was used for *Solanum pennellii* (Sopen) sequences. Trichome-enriched expression data (based on RNA-seq) for sequences in five other species were obtained from Ning et al., 2015 (Solyc= *S. lycopersicum*) and Moghe et al., 2017 (SN= *S. nigrum*; SQ= *S. quitoense*; HN= *Hyoscyamus niger*; SS= *Salpiglossis sinuata*). Peaxi= *Petunia axillaris*; CA= *Capsicum annuum*; Nt= *Nicotiana tabacum*.

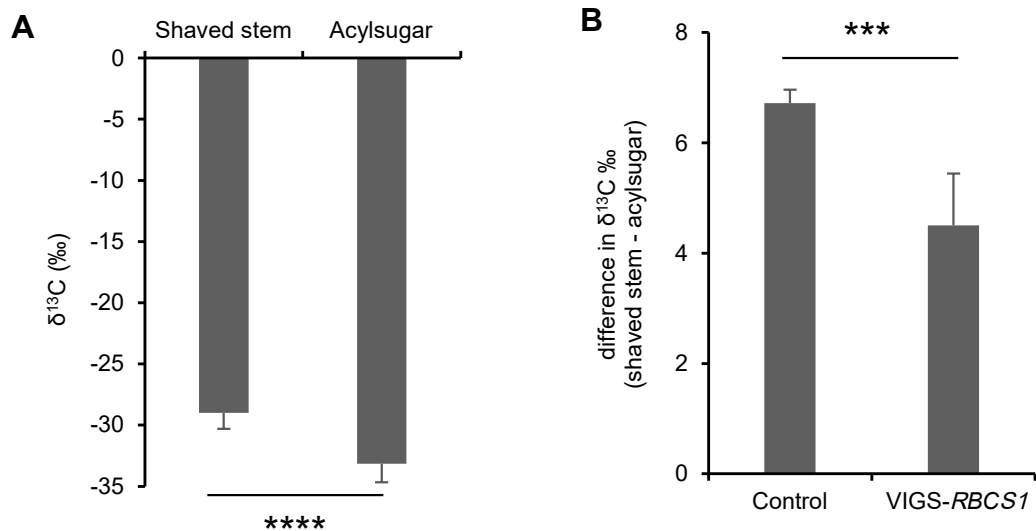


**Figure 6**  $\delta^{13}\text{C}$  analyses. A, Difference in  $\delta^{13}\text{C}$  values between shaved stems and secreted acylsugars. Error bars indicate SE ( $n = 10$  individual plants; \*\*\*\*  $P < 0.0001$ ; Welch  $t$ -test). B, VIGS of *SpRBCS1* reduces the difference in  $\delta^{13}\text{C}$  values between shaved stems and acylsugars. Error bars indicate SE ( $n = 5$  and  $10$  individual plants for control and VIGS-*RBCS1* groups, respectively; \*\*\*  $P < 0.001$ ; Welch  $t$ -test).

## Parsed Citations

**Alba JM, Montserrat M, Fernandez-Munoz R (2009) Resistance to the two-spotted spider mite (*Tetranychus urticae*) by acylsucroses of wild tomato (*Solanum pimpinellifolium*) trichomes studied in a recombinant inbred line population. *Exp Appl Acarol* 47: 35-47**

Google Scholar: [Author Only](#) [Title Only](#) [Author and Title](#)

**Anders S, Pyl PT, Huber W (2015) HTSeq-a Python framework to work with high-throughput sequencing data. *Bioinformatics* 31: 166-169**

Google Scholar: [Author Only](#) [Title Only](#) [Author and Title](#)

**Asai T, Hara N, Fujimoto Y (2010) Fatty acid derivatives and dammarane triterpenes from the glandular trichome exudates of *Ibicella lutea* and *Proboscidea louisiana*. *Phytochemistry* 71: 877-894**

Google Scholar: [Author Only](#) [Title Only](#) [Author and Title](#)

**Asai T, Nakamura Y, Hirayama Y, Ohyama K, Fujimoto Y (2012) Cyclic glycolipids from glandular trichome exudates of *Cerastium glomeratum*. *Phytochemistry* 82: 149-157**

Google Scholar: [Author Only](#) [Title Only](#) [Author and Title](#)

**Balcke GU, Bennewitz S, Bergau N, Athmer B, Henning A, Majovsky P, Jiménez-Gómez JM, Hoehenwarter W, Tissier A (2017) Multi-omics of tomato glandular trichomes reveals distinct features of central carbon metabolism supporting high productivity of specialized metabolites. *Plant Cell* 29: 960-983**

Google Scholar: [Author Only](#) [Title Only](#) [Author and Title](#)

**Ben-Mahmoud S, Smeda JR, Chappell TM, Stafford-Banks C, Kaplinsky CH, Anderson T, Mutschler MA, Kennedy GG, Ullman DE (2018) Acylsugar amount and fatty acid profile differentially suppress oviposition by western flower thrips, *Frankliniella occidentalis*, on tomato and interspecific hybrid flowers. *PLoS One* 13: e0201583**

Google Scholar: [Author Only](#) [Title Only](#) [Author and Title](#)

**Bolger A, Scossa F, Bolger ME, Lanz C, Maumus F, Tohge T, Quesneville H, Aseekh S, Sorensen I, Lichtenstein G, Fich EA, Conte M, Keller H, Schneeberger K, Schwacke R, Ofner I, Vrebalov J, Xu Y, Osorio S, Aflitos SA, Schijlen E, Jimenez-Gomez JM, Rynhajilo M, Kimura S, Kumar R, Koenig D, Headland LR, Maloof JN, Sinha N, van Ham RC, Lankhorst RK, Mao L, Vogel A, Arsova B, Panstruga R, Fei Z, Rose JK, Zamir D, Carrari F, Giovannoni JJ, Weigel D, Usadel B, Fernie AR (2014) The genome of the stress-tolerant wild tomato species *Solanum pennellii*. *Nat Genet* 46: 1034-1038**

Google Scholar: [Author Only](#) [Title Only](#) [Author and Title](#)

**Bolger AM, Lohse M, Usadel B (2014) Trimmomatic: a flexible trimmer for Illumina sequence data. *Bioinformatics* 30: 2114-2120**

Google Scholar: [Author Only](#) [Title Only](#) [Author and Title](#)

**Bonierbale MW, Plaisted RL, Pineda O, Tanksley SD (1994) QTL analysis of trichome-mediated insect resistance in potato. *Theor Appl Genet* 87: 973-987**

Google Scholar: [Author Only](#) [Title Only](#) [Author and Title](#)

**Dong Y, Burch-Smith TM, Liu Y, Mamillapalli P, Dinesh-Kumar SP (2007) A ligation-independent cloning tobacco rattle virus vector for high-throughput virus-induced gene silencing identifies roles for NbMADS4-1 and -2 in floral development. *Plant Physiol* 145: 1161-1170**

Google Scholar: [Author Only](#) [Title Only](#) [Author and Title](#)

**Fan P, Miller AM, Schillmiller AL, Liu X, Ofner I, Jones AD, Zamir D, Last RL (2016) In vitro reconstruction and analysis of evolutionary variation of the tomato acylsucrose metabolic network. *Proc Natl Acad Sci USA* 113: E239-248**

Google Scholar: [Author Only](#) [Title Only](#) [Author and Title](#)

**Fan P, Wang P, Lou YR, Leong BJ, Moore BM, Schenck CA, Combs R, Cao P, Brandizzi F, Shiu SH, Last RL (2020) Evolution of a plant gene cluster in Solanaceae and emergence of metabolic diversity. *eLife* 9: e56717**

Google Scholar: [Author Only](#) [Title Only](#) [Author and Title](#)

**Feng H, Acosta-Gamboa L, Kruse LH, Tracy JD, Chung SH, Nava Ferreira AR, Shakir S, Xu H, Sunter G, Gore MA, Casteel CL, Moghe GD, Jander G (2021) Acylsugars protect *Nicotiana benthamiana* against insect herbivory and desiccation. *Plant Mol Biol* 109: 505-522**

Google Scholar: [Author Only](#) [Title Only](#) [Author and Title](#)

**Fobes JF, Mudd JB, Marsden MP (1985) Epicuticular lipid accumulation on the leaves of *Lycopersicon pennellii* (Corr.) D'Arcy and *Lycopersicon esculentum* Mill. *Plant Physiol* 77: 567-570**

Google Scholar: [Author Only](#) [Title Only](#) [Author and Title](#)

**Guan X, Okazaki Y, Zhang R, Saito K, Nikolau BJ (2020) Dual-localized enzymatic components constitute the Fatty acid synthase systems in mitochondria and plastids. *Plant Physiol* 183: 517-529**

Google Scholar: [Author Only](#) [Title Only](#) [Author and Title](#)

**Kalyaanamoorthy S, Minh BQ, Wong TKF, von Haeseler A, Jermin LS (2017) ModelFinder: fast model selection for accurate**

phylogenetic estimates. *Nat Methods* 14: 587-589

Google Scholar: [Author Only](#) [Title Only](#) [Author and Title](#)

Katoh K, Standley DM (2013) MAFFT multiple sequence alignment software version 7: improvements in performance and usability. *Mol Biol Evol* 30: 772-780

Google Scholar: [Author Only](#) [Title Only](#) [Author and Title](#)

Kavanagh KL, Jornvall H, Persson B, Oppermann U (2008) Medium- and short-chain dehydrogenase/reductase gene and protein families : the SDR superfamily: functional and structural diversity within a family of metabolic and regulatory enzymes. *Cell Mol Life Sci* 65: 3895-3906

Google Scholar: [Author Only](#) [Title Only](#) [Author and Title](#)

Kim D, Pertea G, Trapnell C, Pimentel H, Kelley R, Salzberg SL (2013) TopHat2: accurate alignment of transcriptomes in the presence of insertions, deletions and gene fusions. *Genome Biol* 14

Google Scholar: [Author Only](#) [Title Only](#) [Author and Title](#)

Kim J, Matsuba Y, Ning J, Schillmiller AL, Hammar D, Jones AD, Pichersky E, Last RL (2014) Analysis of natural and induced variation in tomato glandular trichome flavonoids identifies a gene not present in the reference genome. *Plant Cell* 26: 3272-3285

Google Scholar: [Author Only](#) [Title Only](#) [Author and Title](#)

Krause ST, Liao P, Crocoll C, Boachon B, Forster C, Leidecker F, Wiese N, Zhao D, Wood JC, Buell CR, Gershenzon J, Dudareva N, Degenhardt J (2021) The biosynthesis of thymol, carvacrol, and thymohydroquinone in Lamiaceae proceeds via cytochrome P450s and a short-chain dehydrogenase. *Proc Natl Acad Sci USA* 118

Google Scholar: [Author Only](#) [Title Only](#) [Author and Title](#)

Kroumova AB, Wagner GJ (2003) Different elongation pathways in the biosynthesis of acyl groups of trichome exudate sugar esters from various solanaceous plants. *Planta* 216: 1013-1021

Google Scholar: [Author Only](#) [Title Only](#) [Author and Title](#)

Kroumova AB, Zaitlin D, Wagner GJ (2016) Natural variability in acyl moieties of sugar esters produced by certain tobacco and other Solanaceae species. *Phytochem* 130: 218-227

Google Scholar: [Author Only](#) [Title Only](#) [Author and Title](#)

Kumar S, Stecher G, Li M, Knyaz C, Tamura K (2018) MEGAX: Molecular evolutionary genetics analysis across computing platforms. *Mol Biol Evol* 35: 1547-1549

Google Scholar: [Author Only](#) [Title Only](#) [Author and Title](#)

Lattere R, Pottier M, Remacle C, Boutry M (2017) Photosynthetic trichomes contain a specific Rubisco with a modified pH-dependent activity. *Plant Physiol* 173: 2110-2120

Google Scholar: [Author Only](#) [Title Only](#) [Author and Title](#)

Lawson DM, Lunde CF, Mutschler MA (1997) Marker-assisted transfer of acylsugar-mediated pest resistance from the wild tomato, *Lycopersicon pennellii*, to the cultivated tomato, *Lycopersicon esculentum*. *Mol Breeding* 3: 307-317

Google Scholar: [Author Only](#) [Title Only](#) [Author and Title](#)

Leckie BM, D'Ambrosio DA, Chappell TM, Halitschke R, De Jong DM, Kessler A, Kennedy GG, Mutschler MA (2016) Differential and synergistic functionality of acylsugars in suppressing oviposition by insect herbivores. *PLoS One* 11: e0153345

Google Scholar: [Author Only](#) [Title Only](#) [Author and Title](#)

Leckie BM, De Jong DM, Mutschler MA (2012) Quantitative trait loci increasing acylsugars in tomato breeding lines and their impacts on silverleaf whiteflies. *Mol Breeding* 30: 1621-1634

Google Scholar: [Author Only](#) [Title Only](#) [Author and Title](#)

Lou YR, Anthony TM, Fiesel PD, Arking RE, Christensen EM, Jones AD, Last RL (2021) It happened again: Convergent evolution of acylglucose specialized metabolism in black nightshade and wild tomato. *Sci Adv* 7: eabj8726

Google Scholar: [Author Only](#) [Title Only](#) [Author and Title](#)

Luu VT, Weinhold A, Ullah C, Dressel S, Schoettner M, Gase K, Gaquere E, Xu S, Baldwin IT (2017) O-acyl sugars protect a wild tobacco from both native fungal pathogens and a specialist herbivore. *Plant Physiol* 174: 370-386

Google Scholar: [Author Only](#) [Title Only](#) [Author and Title](#)

Mandal S, Ji W, McKnight TD (2020) Candidate gene networks for acylsugar metabolism and plant defense in wild tomato *Solanum pennellii*. *Plant Cell* 32: 81-99

Google Scholar: [Author Only](#) [Title Only](#) [Author and Title](#)

Mazourek M, Pujar A, Borovsky Y, Paran I, Mueller L, Jahn MM (2009) A dynamic interface for capsaicinoid systems biology. *Plant Physiol* 150: 1806-1821

Google Scholar: [Author Only](#) [Title Only](#) [Author and Title](#)

McDermott EG, Mullens BA, Mayo CE, Roark EB, Maupin CR, Gerry AC, Hamer GL (2019) Laboratory evaluation of stable isotope

labeling of *Culicoides* (Diptera: Ceratopogonidae) for adult dispersal studies. *Parasit Vectors* 12: 411

Google Scholar: [Author Only](#) [Title Only](#) [Author and Title](#)

Minh BQ, Schmidt HA, Chernomor O, Schrepf D, Woodhams MD, von Haeseler A, Lanfear R (2020) IQ-TREE 2: New models and efficient methods for phylogenetic inference in the genomic era. *Mol Biol Evol* 37: 1530-1534

Google Scholar: [Author Only](#) [Title Only](#) [Author and Title](#)

Moghe GD, Last RL (2015) Something old, something new: Conserved enzymes and the evolution of novelty in plant specialized metabolism. *Plant Physiol* 169: 1512-1523

Google Scholar: [Author Only](#) [Title Only](#) [Author and Title](#)

Moghe GD, Leong BJ, Hurney SM, Daniel Jones A, Last RL (2017) Evolutionary routes to biochemical innovation revealed by integrative analysis of a plant-defense related specialized metabolic pathway. *eLife* 6: e28468

Google Scholar: [Author Only](#) [Title Only](#) [Author and Title](#)

Moore BM, Wang P, Fan P, Leong B, Schenck CA, Lloyd JP, Lehti-Shiu MD, Last RL, Pichersky E, Shiu SH (2019) Robust predictions of specialized metabolism genes through machine learning. *Proc Natl Acad Sci USA* 116: 2344-2353

Google Scholar: [Author Only](#) [Title Only](#) [Author and Title](#)

Morita K, Hatanaka T, Misoo S, Fukayama H (2014) Unusual small subunit that is not expressed in photosynthetic cells alters the catalytic properties of Rubisco in rice. *Plant Physiol* 164: 69-79

Google Scholar: [Author Only](#) [Title Only](#) [Author and Title](#)

Nadakuduti SS, Uebler JB, Liu X, Jones AD, Barry CS (2017) Characterization of trichome-expressed BAHD acyltransferases in *Petunia axillaris* reveals distinct acylsugar assembly mechanisms within the Solanaceae. *Plant Physiol* 175: 36-50

Google Scholar: [Author Only](#) [Title Only](#) [Author and Title](#)

Ning J, Moghe GD, Leong B, Kim J, Ofner I, Wang Z, Adams C, Jones AD, Zamir D, Last RL (2015) A feedback-insensitive isopropylmalate synthase affects acylsugar composition in cultivated and wild tomato. *Plant Physiol* 169: 1821-1835

Google Scholar: [Author Only](#) [Title Only](#) [Author and Title](#)

Okamoto S, Yu F, Harada H, Okajima T, Hattan J, Misawa N, Utsumi R (2011) A short-chain dehydrogenase involved in terpene metabolism from *Zingiber zerumbet*. *FEBS J* 278: 2892-2900

Google Scholar: [Author Only](#) [Title Only](#) [Author and Title](#)

Polichuk DR, Zhang Y, Reed DW, Schmidt JF, Covello PS (2010) A glandular trichome-specific monoterpene alcohol dehydrogenase from *Artemisia annua*. *Phytochemistry* 71: 1264-1269

Google Scholar: [Author Only](#) [Title Only](#) [Author and Title](#)

Ringer KL, Davis EM, Croteau R (2005) Monoterpene metabolism. Cloning, expression, and characterization of (-)-isopiperitenol/(-)-carveol dehydrogenase of peppermint and spearmint. *Plant Physiol* 137: 863-872

Google Scholar: [Author Only](#) [Title Only](#) [Author and Title](#)

Robinson MD, McCarthy DJ, Smyth GK (2010) edgeR: a Bioconductor package for differential expression analysis of digital gene expression data. *Bioinformatics* 26: 139-140

Google Scholar: [Author Only](#) [Title Only](#) [Author and Title](#)

Sakai T, Tanemura Y, Itoh S, Fujimoto Y (2013) Dodecyl alpha-L-rhamnopyranosyl-(1->2)-beta-D-fucopyranoside derivatives from the glandular trichome exudate of *Erodium pelargoniflorum*. *Chem Biodivers* 10: 1099-1108

Google Scholar: [Author Only](#) [Title Only](#) [Author and Title](#)

Schillmiller AL, Gilgallon K, Ghosh B, Jones AD, Last RL (2016) Acylsugar acylhydrolases: Carboxylesterase-catalyzed hydrolysis of acylsugars in tomato trichomes. *Plant Physiol* 170: 1331-1344

Google Scholar: [Author Only](#) [Title Only](#) [Author and Title](#)

Schillmiller AL, Moghe GD, Fan P, Ghosh B, Ning J, Jones AD, Last RL (2015) Functionally divergent alleles and duplicated loci encoding an acyltransferase contribute to acylsugar metabolite diversity in *Solanum* trichomes. *Plant Cell* 27: 1002-1017

Google Scholar: [Author Only](#) [Title Only](#) [Author and Title](#)

Severson RF, Johnson AW, Jackson DM (1985) Cuticular constituents of tobacco: factors affecting their production and their role in insect and disease resistance and smoke quality. *Recent Advances in Tobacco Science* 11: 105-173

Google Scholar: [Author Only](#) [Title Only](#) [Author and Title](#)

Shimura K, Okada A, Okada K, Jikumaru Y, Ko KW, Toyomasu T, Sassa T, Hasegawa M, Kodama O, Shibuya N, Koga J, Nojiri H, Yamane H (2007) Identification of a biosynthetic gene cluster in rice for momilactones. *J Biol Chem* 282: 34013-34018

Google Scholar: [Author Only](#) [Title Only](#) [Author and Title](#)

Slocombe SP, Schauvinhold I, McQuinn RP, Besser K, Welsby NA, Harper A, Aziz N, Li Y, Larson TR, Giovannoni J, Dixon RA, Broun P (2008) Transcriptomic and reverse genetic analyses of branched-chain fatty acid and acyl sugar production in *Solanum pennellii* and *Nicotiana benthamiana*. *Plant Physiol* 148: 1830-1846

Google Scholar: [Author Only](#) [Title Only](#) [Author and Title](#)

**Smith BN, Epstein S (1971) Two categories of c/c ratios for higher plants. Plant Physiol 47: 380-384**

Google Scholar: [Author Only](#) [Title Only](#) [Author and Title](#)

**Sonawane PD, Heinig U, Panda S, Gilboa NS, Yona M, Kumar SP, Alkan N, Unger T, Bocobza S, Pliner M, Malitsky S, Tkachev M, Meir S, Rogachev I, Aharoni A (2018) Short-chain dehydrogenase/reductase governs steroidal specialized metabolites structural diversity and toxicity in the genus Solanum. Proc Natl Acad Sci USA 115: E5419-E5428**

Google Scholar: [Author Only](#) [Title Only](#) [Author and Title](#)

**Stewart C, Jr., Kang BC, Liu K, Mazourek M, Moore SL, Yoo EY, Kim BD, Paran I, Jahn MM (2005) The PUN1 gene for pungency in pepper encodes a putative acyltransferase. Plant J 42: 675-688**

Google Scholar: [Author Only](#) [Title Only](#) [Author and Title](#)

**Suyama M, Torrents D, Bork P (2006) PAL2NAL: robust conversion of protein sequence alignments into the corresponding codon alignments. Nucleic Acids Res 34: W609-612**

Google Scholar: [Author Only](#) [Title Only](#) [Author and Title](#)

**Tomato Genome C (2012) The tomato genome sequence provides insights into fleshy fruit evolution. Nature 485: 635-641**

Google Scholar: [Author Only](#) [Title Only](#) [Author and Title](#)

**Walters DS, Steffens JC (1990) Branched chain amino acid metabolism in the biosynthesis of Lycopersicon pennellii glucose esters. Plant Physiol 93: 1544-1551**

Google Scholar: [Author Only](#) [Title Only](#) [Author and Title](#)

**Weinhold A, Baldwin IT (2011) Trichome-derived O-acyl sugars are a first meal for caterpillars that tags them for predation. Proc Natl Acad Sci USA 108: 7855-7859**

Google Scholar: [Author Only](#) [Title Only](#) [Author and Title](#)

**Yang Z (1997) PAML: a program package for phylogenetic analysis by maximum likelihood. Comput Appl Biosci 13: 555-556**

Google Scholar: [Author Only](#) [Title Only](#) [Author and Title](#)

**Yang Z, Nielsen R (2000) Estimating synonymous and nonsynonymous substitution rates under realistic evolutionary models. Mol Biol Evol 17: 32-43**

Google Scholar: [Author Only](#) [Title Only](#) [Author and Title](#)